



RESEARCH ARTICLE SUMMARY

CORONAVIRUS

Persistent complement dysregulation with signs of thromboinflammation in active Long Covid

Carlo Cervia-Hasler, Sarah C. Brüningk, Tobias Hoch, Bowen Fan, Giulia Muzio, Ryan C. Thompson, Laura Ceglarek, Roman Meledin, Patrick Westermann, Marc Emmenegger, Patrick Taeschler, Yves Zurbuchen, Michele Pons, Dominik Menges, Tala Ballouz, Sara Cervia-Hasler, Sarah Adamo, Miriam Merad, Alexander W. Charney, Milo Puhan, Petter Brodin, Jakob Nilsson, Adriano Aguzzi, Miro E. Raeber, Christoph B. Messner, Noam D. Beckmann, Karsten Borgwardt, Onur Boyman*

INTRODUCTION: Acute infection with severe acute respiratory syndrome coronavirus 2 (SARS-CoV-2) causes various clinical phenotypes, ranging from asymptomatic to life-threatening COVID-19. About 5% of all infected individuals do not recover from acute disease but develop long-term complications, called Long Covid. Current hypotheses on factors contributing to Long Covid include tissue damage, viral reservoirs, autoimmunity, and persistent inflammation. There are currently no diagnostic tests or therapeutic solutions for affected patients.

RATIONALE: We followed 39 healthy controls and 113 COVID-19 patients for up to 1 year after initial confirmation of acute SARS-CoV-2 infection to identify biomarkers associated with Long Covid. At 6-month follow-up, 40 patients had Long Covid symptoms. Repeated clinical assessments were paired with blood draws, resulting in a total of 268 longitudinal blood samples. We measured >6500 proteins in serum by proteomics. Top candidate biomarkers were identified using computational tools and further evaluated experimentally.

RESULTS: Long Covid patients exhibited increased complement activation during acute disease, which also persisted at 6-month follow-up. The complement system is part of the innate immune system and contributes to immunity and homeostasis by targeting pathogens and damaged cells, among other functions. Interestingly, blood complement levels normalized in Long Covid patients recovering before their 6-month follow-up. The complement system can be activated by various triggers, resulting in formation of the terminal complement complex (TCC), made of the complement components C5b-9. These complexes can integrate into cell membranes and induce cell activation or lysis. Long Covid patients showed imbalanced TCC formation, marked by increased soluble C5bC6 complexes and decreased levels of C7-containing TCC formations that can incorporate into cell membranes. This suggested increased membrane insertion of TCCs in Long Covid patients, contributing to tissue damage. Accordingly, Long Covid patients showed elevated tissue injury markers in blood and a thromboinflammatory signature, char-

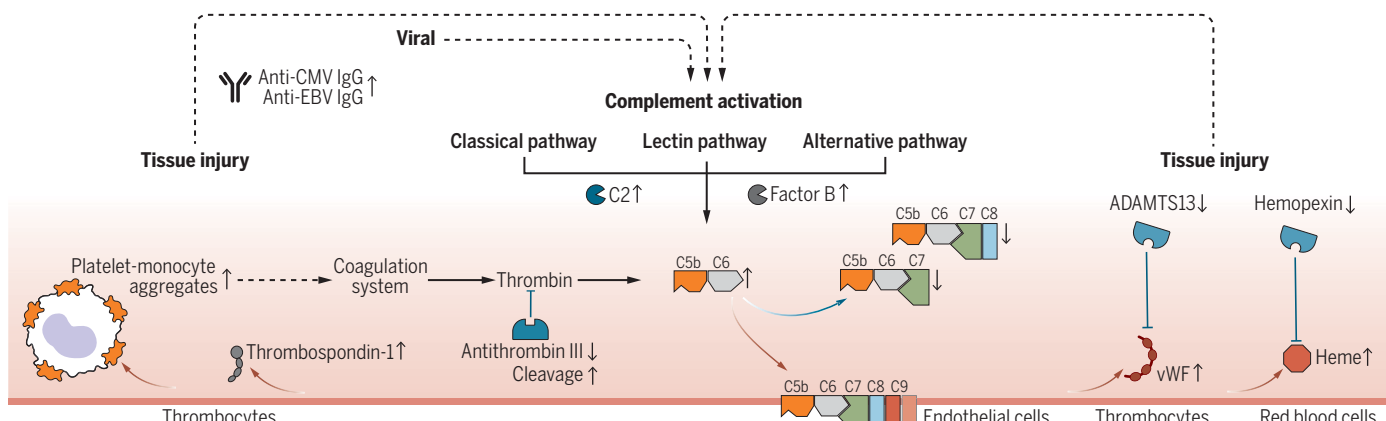
acterized by markers of endothelial activation such as von Willebrand factor (vWF), and blood cell lysis. Low antithrombin III levels in Long Covid patients were accompanied by signs of increased cleavage by thrombin, a driver of TCC formation. Furthermore, Long Covid patients had elevated platelet activation markers and monocyte-platelet aggregates at 6-month follow-up, particularly in cases where Long Covid persisted for 12 months or more. These patients also showed signs of antibody-mediated activation of the classical complement pathway, which was associated with increased anti-CMV (cytomegalovirus, also known as human herpesvirus 5) and anti-EBV (Epstein-Barr virus) immunoglobulin G (IgG) antibody levels.

CONCLUSION: Our data suggest that active Long Covid is accompanied by a blood protein signature marked by increased complement activation and thromboinflammation, including activated platelets and markers of red blood cell lysis. Tissue injury may also be complement-mediated and, in turn, activate the complement system. Moreover, complement activation may be driven by antigen-antibody complexes, involving autoantibodies and antibodies against herpesviruses, as well as cross-talk with a dysregulated coagulation system. In addition to offering a basis for new diagnostic solutions, our work provides support for clinical research on complement modulators for patients suffering from Long Covid. ■

The list of author affiliations is available in the full article online.

*Corresponding author. Email: onur.boyman@uzh.ch
Cite this article as C. Cervia-Hasler et al., *Science* **383**, eadg7942 (2024). DOI: 10.1126/science.adg7942

S READ THE FULL ARTICLE AT
<https://doi.org/10.1126/science.adg7942>



Pathomechanistic model of Long Covid. Model of complement-mediated thromboinflammation, showing increased and decreased biomarkers (up arrows and down arrows, respectively) measured at 6-month follow-up in patients with persistent Long Covid symptoms compared with recovered COVID-19 patients and healthy controls. Measurements were done using proteomics, spectral flow cytometry, single-cell transcriptomics, high-throughput antibody measurements, and targeted assays. Red arrows mark activating protein interactions, and blue arrows mark inhibiting protein interactions. Dashed arrows connect changes in different biological pathways.

RESEARCH ARTICLE

CORONAVIRUS

Persistent complement dysregulation with signs of thromboinflammation in active Long Covid

Carlo Cervia-Hasler¹, Sarah C. Brüning^{2,3}, Tobias Hoch¹, Bowen Fan^{2,3}, Giulia Muzio^{2,3}, Ryan C. Thompson^{4,5,6}, Laura Ceglarek¹, Roman Meledin¹, Patrick Westermann⁷, Marc Emmenegger⁸, Patrick Taeschler¹, Yves Zurbuchen¹, Michele Pons¹, Dominik Menges⁹, Tala Ballouz⁹, Sara Cervia-Hasler¹, Sarah Adamo¹, Miriam Merad⁴, Alexander W. Charney^{4,5,6}, Milo Puhan⁹, Petter Brodin^{10,11}, Jakob Nilsson¹, Adriano Aguzzi⁸, Miro E. Raeber¹, Christoph B. Messner⁷, Noam D. Beckmann^{4,5,6,12}, Karsten Borgwardt^{2,3}, Onur Boyman^{1,13*}

Long Covid is a debilitating condition of unknown etiology. We performed multimodal proteomics analyses of blood serum from COVID-19 patients followed up to 12 months after confirmed severe acute respiratory syndrome coronavirus 2 infection. Analysis of >6500 proteins in 268 longitudinal samples revealed dysregulated activation of the complement system, an innate immune protection and homeostasis mechanism, in individuals experiencing Long Covid. Thus, active Long Covid was characterized by terminal complement system dysregulation and ongoing activation of the alternative and classical complement pathways, the latter associated with increased antibody titers against several herpesviruses possibly stimulating this pathway. Moreover, markers of hemolysis, tissue injury, platelet activation, and monocyte–platelet aggregates were increased in Long Covid. Machine learning confirmed complement and thromboinflammatory proteins as top biomarkers, warranting diagnostic and therapeutic interrogation of these systems.

Acute infection with severe acute respiratory syndrome coronavirus 2 (SARS-CoV-2) causes a variety of clinical phenotypes ranging from asymptomatic to life-threatening COVID-19 (1). Continuous transmission of SARS-CoV-2 in a previously naïve population has been accompanied by mounting evidence that about 20% of patients diagnosed with COVID-19 and about 5% of all SARS-CoV-2-infected persons do not recover from acute disease but develop long-term complications, called Long Covid (2–4). Multifaceted symptoms, including fatigue, post-

exertional malaise, and cognitive impairment (5), can resemble other postviral conditions and myalgic encephalomyelitis/chronic fatigue syndrome (ME/CFS) (6). Current hypotheses on Long Covid include tissue damage, viral reservoirs, autoimmunity, and persistent inflammation (7).

The immune response to SARS-CoV-2 has been extensively studied and is initiated at first contact with the virus, leading to strong activation of the innate and adaptive immune systems (8–12). These include interferons and immunoglobulin G3 (IgG3), the latter an IgG subset involved in antiviral immune responses and considered a protective factor against Long Covid and ME/CFS (13–15). Acute SARS-CoV-2-related immunopathology has been associated with excess inflammation, complement activation, hypercoagulation, and vascular injury (16, 17). We applied two high-throughput proteomics approaches to a prospective cohort that included healthy controls, Long Covid patients, and patients who fully recovered from mild or severe COVID-19. Based on longitudinal measurements of >6500 serum proteins, we found evidence of persistent complement-mediated immunopathology associated with thromboinflammation in individuals experiencing Long Covid.

Results

Cohort characteristics

In this multicenter study, we followed 113 COVID-19 patients for up to 1 year. Study participants were included after confirmed acute

SARS-CoV-2 infection, determined by a reverse transcriptase quantitative polymerase chain reaction (RT-qPCR) test, and were seen for follow-up visits at 6 and 12 months after acute COVID-19. Moreover, 39 healthy adults were included as controls (fig. S1A and table S1). Of the 113 COVID-19 patients, 37 (33%) had a disease course classified as severe according to the World Health Organization (WHO) criteria (1, 18). Sixty-five patients (58%) recovered fully, whereas 48 patients reported one or more COVID-19-related symptoms that persisted at 6-month follow-up (hereafter referred to as 6-month Long Covid). Eight patients indicated only changes in smell or taste; as isolated chemosensory disorders may reflect only a local pathology of the olfactory system (19), we excluded these individuals from our 6-month Long Covid definition. Therefore, we used samples from 40 patients to investigate systemic mechanisms underlying Long Covid. The 6-month Long Covid group showed a higher prevalence of severe acute COVID-19 compared with the 73 other COVID-19 patients (table S1). Sixteen patients without 6-month Long Covid experienced symptoms for longer than 1 month but recovered before the 6-month follow-up (Fig. 1A). In the 12-month follow-up, 22 of the 40 6-month Long Covid patients reported persisting symptoms, whereas 10 had recovered and 8 were lost to follow-up (fig. S1A).

Serum proteome of patients with persistent Long Covid at 6-month follow-up

Serum was collected from healthy controls and COVID-19 patients during acute COVID-19 and at 6-month follow-up. To analyze serum proteins, we used the SomaScan platform (20). This platform is based on synthetic aptamers that are short single-stranded nucleic acids with unique binding specificities to proteins, similar to antibodies. The platform included 7289 different aptamers targeting distinct human protein epitopes. As some proteins were targeted by several aptamers, a total of 6596 different human proteins were measured (Fig. 1A). We detected differences in serum protein levels between patients with severe COVID-19 and those with mild acute COVID-19 (Fig. 1B), as well as differences between 6-month Long Covid patients and patients without 6-month Long Covid (Fig. 1C), both during acute COVID-19 and at 6-month follow-up.

Severe COVID-19 is associated with autoantibody formation and persistent inflammation even after recovery (21–24) and thus can confound Long Covid-associated changes. We therefore searched for differences in the serum proteome that were distinct from those related to severe COVID-19. To this end, we tested all aptamer measurements for association with 6-month Long Covid, while considering potential confounders, such as patient age, sex, and hospitalization status (13, 25). Statistical

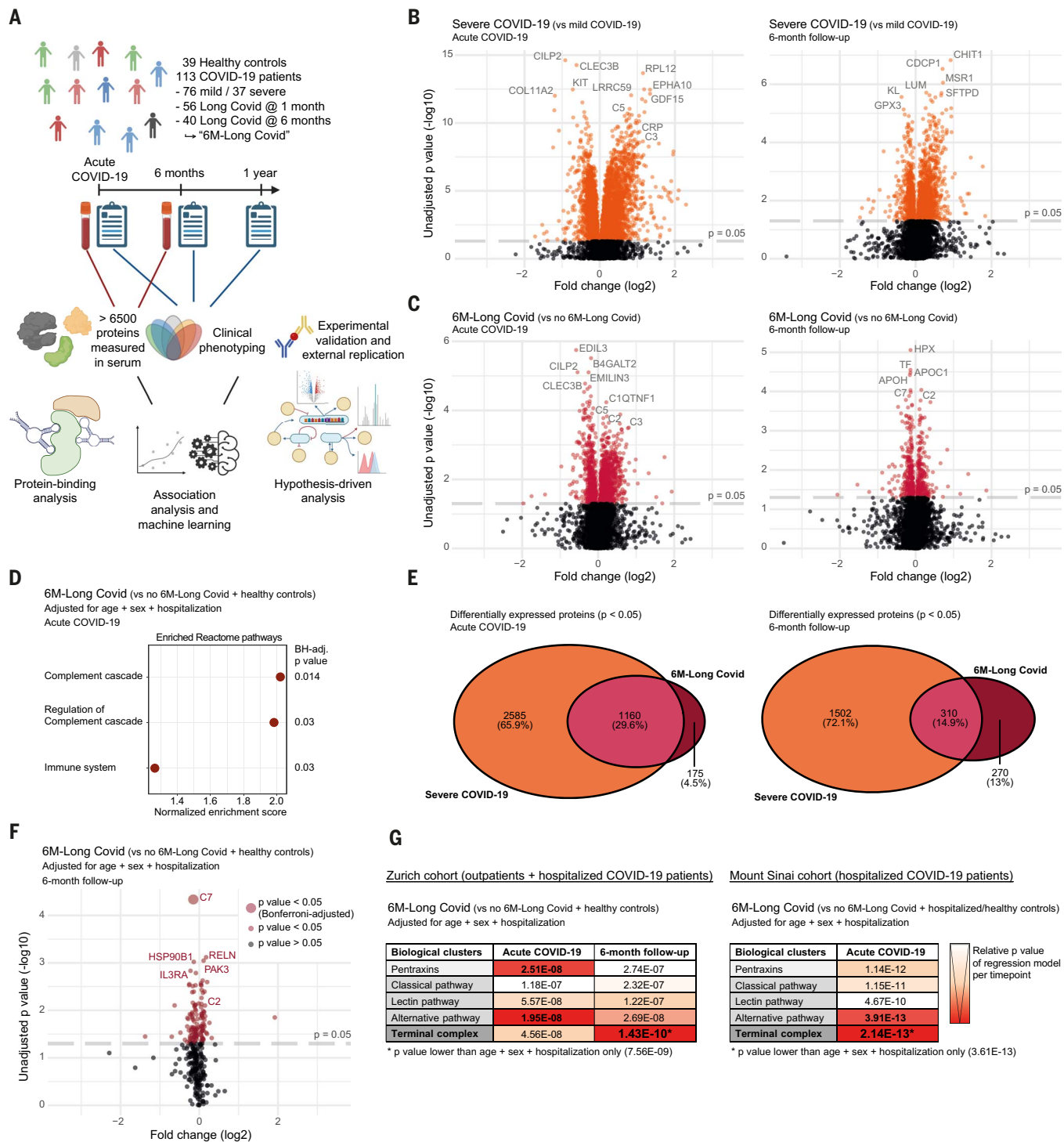
¹Department of Immunology, University Hospital Zurich, University of Zurich, 8091 Zurich, Switzerland. ²Department of Biosystems Science and Engineering, ETH Zurich, 4058 Basel, Switzerland. ³Swiss Institute of Bioinformatics, 1015 Lausanne, Switzerland. ⁴Icahn School of Medicine at Mount Sinai, New York, NY 10029, USA. ⁵Charles Bronfman Institute for Personalized Medicine, Icahn School of Medicine at Mount Sinai, New York, NY 10029, USA. ⁶Mount Sinai Clinical Intelligence Center, Icahn School of Medicine at Mount Sinai, New York, NY 10029, USA. ⁷Precision Proteomics Center, Swiss Institute of Allergy and Asthma Research, University of Zurich, 7265 Davos, Switzerland.

⁸Institute of Neuropathology, University Hospital Zurich, University of Zurich, 8091 Zurich, Switzerland.

⁹Epidemiology, Biostatistics and Prevention Institute, University of Zurich, 8001 Zurich, Switzerland. ¹⁰Unit for Clinical Pediatrics, Department of Women's and Children's Health, Karolinska Institute, 17165 Solna, Sweden.

¹¹Department of Immunology and Inflammation, Imperial College London, London W12 0NN, UK. ¹²Division of Data Driven and Digital Medicine (D3M), Department of Medicine, Icahn School of Medicine at Mount Sinai, New York, NY 10029, USA. ¹³Faculty of Medicine and Faculty of Science, University of Zurich, 8006 Zurich, Switzerland.

*Corresponding author. Email: onur.boyman@uzh.ch

**Fig. 1. Differentially expressed proteins and pathways in Long Covid.**

(A) Study overview indicating the number of individuals used to generate data. [Created with BioRender.com] (B and C) Volcano plots showing differential serum levels of 7289 human protein epitopes in (B) severe versus mild COVID-19 patients and (C) patients with Long Covid (6-month Long Covid) versus no Long Covid at 6-month follow-up (no 6-month Long Covid), measured during acute COVID-19 (left) and at 6-month follow-up (right), using two-tailed t tests. (D) Significantly enriched Reactome pathways using 6408 different proteins measured during acute COVID-19, ranked by means of logistic regression. Benjamini-Hochberg (BH) adjusted. (E) Venn diagram showing overlap of proteins ($P < 0.05$) in (B) and (C). (F) Volcano plot showing differential expression

of 331 epitopes [from 270 proteins from (E), right] selected at 6-month follow-up. Logistic regression of 6-month Long Covid (versus no 6-month Long Covid and healthy controls) adjusted for patient age, sex, and hospitalization. Bonferroni adjusted. (G) Association of protein clusters (table S2) with 6-month Long Covid (versus no 6-month Long Covid and healthy controls), including covariates patient age, sex, and hospitalization, in the Zurich cohort during acute COVID-19 and at 6-month follow-up (left) and the Mount Sinai cohort during acute COVID-19 (right; $n = 280$, including 145 6-month Long Covid patients). P values were calculated using logistic regression with likelihood-ratio test, colored according to their relative value at each time point (columns) and highlighted with asterisks when lower than a regression model based on covariates only.

modeling was applied to data of patients with 6-month Long Covid, patients without 6-month Long Covid, and healthy controls. The association between individual aptamer measurements, representing protein serum levels, and 6-month Long Covid was quantified for further analysis of enriched biological pathways (26). The pathways “complement cascade,” “regulation of complement cascade,” and “immune system” were significantly enriched in 6-month Long Covid patients during acute COVID-19 (Fig. 1D and fig. S1B) but not at 6-month follow-up (fig. S1C). Next, we compared proteins enriched in severe acute COVID-19 patients with proteins enriched in 6-month Long Covid patients and found a large overlap, particularly during acute COVID-19 (Fig. 1E and data S1 to S4). To identify biomarkers of Long Covid that are also applicable to patients with mild acute disease, we examined proteins that were specific to 6-month Long Covid patients at 6-month follow-up (Fig. 1E) and tested for their association with 6-month Long Covid, while considering patient age, sex, and hospitalization status during acute illness. We found complement component 7 (C7) measurements by one aptamer (seq.2888.49) to be significantly decreased in 6-month Long Covid patients (Fig. 1F).

C7 belongs to the complement system, which is part of the innate immune response and comprises a protein cascade targeting pathogens and cell debris, among other functions. The complement system can be activated by antigen-antibody complexes (classical pathway), bacterial sugars (lectin pathway), or spontaneously on cell surfaces (alternative pathway), requiring regulatory control on host cells. All three pathways lead to cleavage of C5 into C5b, which sequentially binds to C6, C7, C8, and C9, thus forming the terminal complement complex (or TCC; C5b-9). This complex can integrate into cell membranes and mediate cell activation or lysis. Pentraxins, a protein group involved in acute immune reactions, can also activate complement pathways (27, 28).

Based on our finding of decreased C7, we analyzed association of 6-month Long Covid with protein clusters of selected biological pathways related to C7, including other TCC components and upstream complement activation pathways (table S2). Association of the selected pathways with 6-month Long Covid was analyzed, considering patient age, sex, and hospitalization, using logistic regression with likelihood-ratio test. During acute COVID-19, pentraxins and the alternative complement activation pathway were most strongly associated with 6-month Long Covid (Fig. 1G). At 6-month follow-up, TCC components were most differentially expressed in 6-month Long Covid patients, with C7 (measured by two different aptamers) representing the top associated protein cluster within the TCC (Fig. 1G and fig. S1D).

To confirm complement dysregulation in Long Covid, we analyzed SomaScan measurements in acute COVID-19 samples of an independent external cohort (the Mount Sinai cohort), including 198 patients hospitalized due to acute COVID-19, of which 145 (73.2%) developed 6-month Long Covid (fig. S1E and table S3). In the Mount Sinai cohort, TCC components were most differentially expressed in 6-month Long Covid patients, compared with COVID-19 patients without 6-month Long Covid, patients hospitalized for reasons unrelated to COVID-19, and healthy controls, with C5bC6 complexes representing the top associated protein cluster within the TCC during acute COVID-19 (Fig. 1G and fig. S1D). Altogether, we found evidence of a dysregulated complement system in 6-month Long Covid patients, particularly affecting the terminal pathway including C7.

Reduced levels of complement component 7 complexes in active Long Covid

C7 can be found as monomeric protein and as C7 complexes within the TCC formations C5b-7, C5b-8, and C5b-9 (Fig. 2A) (27). Thus, we determined C7 aptamer (seq.2888.49) specificity by an in-house enzyme-linked immunosorbent assay (ELISA) using C7 aptamers to capture different complement components. ELISA confirmed C7 aptamer binding to monomeric and complexed C7 but no other TCC components (fig. S2A). C7 aptamer-based pull-down and ELISA of monomeric and complexed TCC components in the presence of a polyanionic competitor, representing similar conditions as in the SomaScan assay, revealed strong aptamer binding to C7 complexes but not monomeric C7 (fig. S2, B and C), showing increased specificity of the C7 aptamer for complexed C7. Further analysis of C7 aptamer measurements by SomaScan revealed significantly reduced serum C7 complexes in patients with 6-month Long Covid at 6-month follow-up (Fig. 2B, left panel). Notably, C7 complexes were consistently reduced at 6-month follow-up, both in mild and severe cases with 6-month Long Covid (Fig. 2B, right panel). No significant differences could be detected when comparing healthy controls with mild and severe COVID-19 cases (Fig. 2C).

To assess whether C7 complexes were low only in Long Covid patients with active disease, we grouped patients without 6-month Long Covid into patients who recovered within 1 month (no Long Covid) and patients experiencing prolonged symptoms for more than 1 month but who fully recovered from Long Covid before 6-month follow-up (hereafter referred to as recovered Long Covid). Only 6-month Long Covid patients had decreased C7 complexes at 6-month follow-up, whereas recovered Long Covid patients had normal serum levels (Fig. 2D). Paired comparison of acute COVID-19 and 6-month follow-up samples revealed no signifi-

cant changes of C7 levels with time (Fig. 2, E and F). Increasing patient age was not correlated with decreased C7 complexes (fig. S2D). Additionally, COVID-19 vaccination status did not influence the association of low C7 complexes with 6-month Long Covid (fig. S2E and table S4).

As monomeric C7 is 1000 times more abundant than C7 in TCCs in serum (29), we applied an ELISA using polyclonal C7-specific antibodies to quantify total C7. In contrast to the C7 aptamer, polyclonal anti-C7 antibodies target multiple epitopes on C7 and detect both monomeric and complexed C7. Total C7 levels were comparable in individuals with and without 6-month Long Covid, suggesting an isolated decrease in C7 complexes in 6-month Long Covid (Fig. 2G). A second aptamer targeting a different C7 epitope (seq.13731.14) was also unchanged in 6-month Long Covid patients compared with patients without 6-month Long Covid (fig. S2F) and correlated with total C7 levels measured by antibody-based ELISA (fig. S2G), thus most likely recognizing an epitope accessible on monomeric C7. The ratio of C7 complexes (measured by seq.2888.49) over total C7 (measured by seq.13731.14) was consistently decreased in 6-month Long Covid patients at 6-month follow-up (fig. S2H). We did not detect increased C7-specific autoantibody reactivity in 6-month Long Covid patients, suggesting no interference with C7 complex formation by autoantibodies (Fig. 2H and fig. S2, I and J). Thus, we observed low serum levels of C7 complexes in active Long Covid at 6-month follow-up, which normalized upon recovery.

Increased C5bC6 levels and complement activity in Long Covid

Formation of the TCC is initiated by association of C5b and C6 in stable bimolecular C5bC6 complexes. The recruitment of C7 to the C5bC6 complex enables subsequent binding to C8 and multiple C9 molecules, ultimately forming the potentially lytic membrane attack complex (MAC) or soluble C5b-9 (sC5b-9) (27). C7 is a central regulator of this process, as it can either scavenge C5bC6, forming soluble C7 complexes, or incorporate C5bC6 into cell membranes, leading to MAC formation and subsequent target-cell activation or lysis (30, 31). In agreement with previous reports on increased complement activation in severe COVID-19 (32), we observed the highest C5bC6 levels in severe cases of acute COVID-19, which remained elevated at 6-month follow-up (Fig. 3A). In patients with 6-month Long Covid, we found higher C5bC6 levels both during acute COVID-19 and at 6-month follow-up compared with patients without 6-month Long Covid (Fig. 3B) and those who recovered before 6-month follow-up (fig. S3A). Paired comparison of acute COVID-19 and 6-month follow-up samples showed that in 6-month Long Covid patients, C5bC6 levels

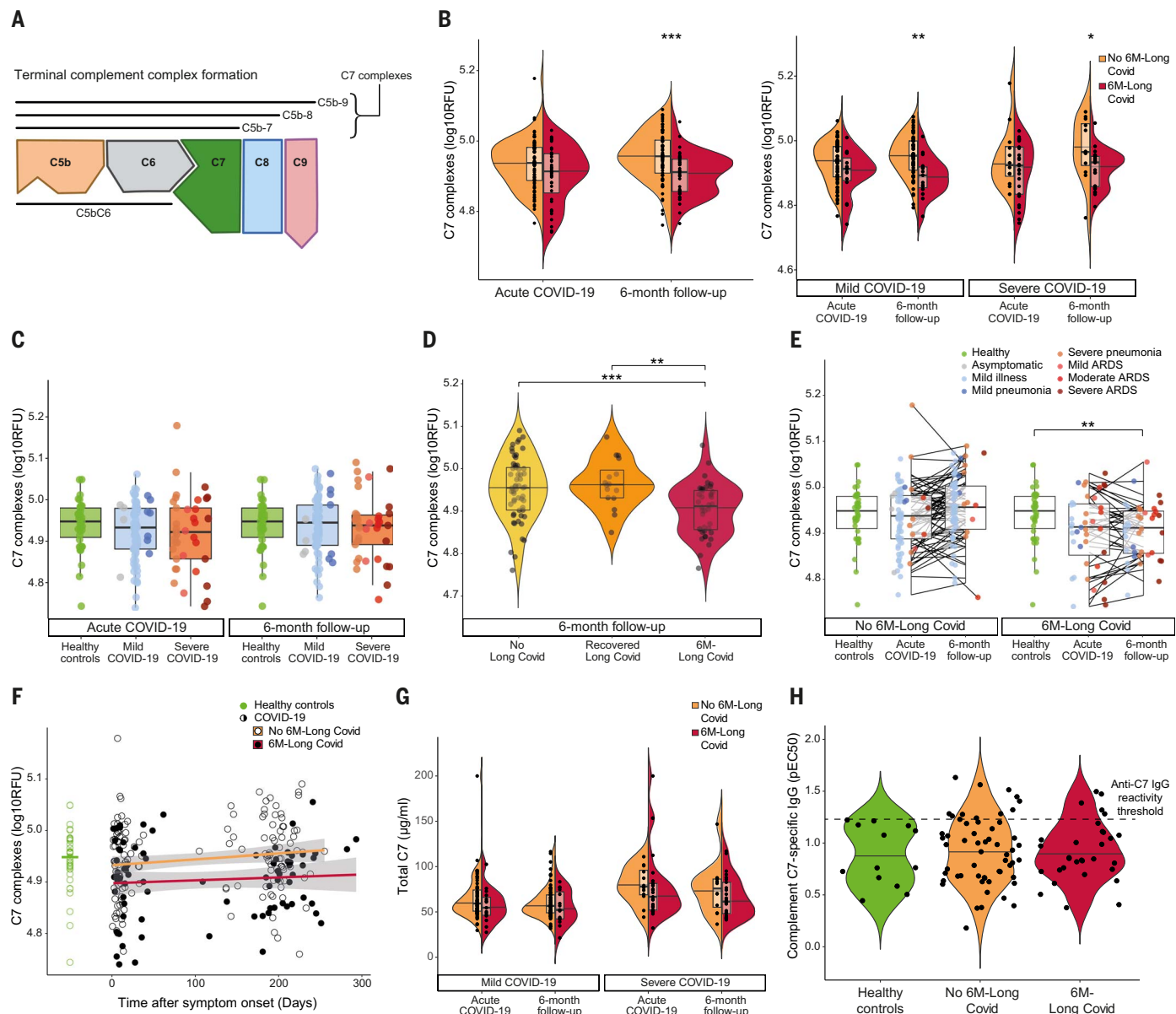


Fig. 2. Reduced levels of complement component 7 complexes in active Long Covid. (A) Schematic of terminal complement complexes. (B) Complement component 7 (C7) complexes in \log_{10} -transformed relative fluorescence units (\log_{10} RFU), measured by C7 aptamer seq.2888.49 in patients without (orange) or with 6-month Long Covid (red), during acute COVID-19 (left) and at 6-month follow-up (right). Comparison of all patients (left panel), and mild versus severe cases (right panel). (C) C7 complexes in healthy controls, mild or severe COVID-19 patients, at acute COVID-19 (left) and 6-month follow-up (right). (D) C7 complexes in patients with no Long Covid (symptom duration < 1 month), Long Covid recovered before 6-month follow-up, or 6-month Long Covid, at 6-month

follow-up. (E) C7 complexes in patients without (left) or with 6-month Long Covid (right), at acute COVID-19 and 6-month follow-up (paired, Wilcoxon signed-rank test), compared with healthy controls. Lines connect corresponding patients. (F) C7 complexes in patients without (open circles) or with 6-month Long Covid (black dots), relative to time after symptom onset, including linear models. Healthy controls with median. (G) Total C7 (ELISA) in mild and severe COVID-19 patients without or with 6-month Long Covid, at acute COVID-19 and 6-month follow-up. (H) C7-specific IgG in healthy controls, patients without or with 6-month Long Covid at 12-month follow-up ($n = 101$), with median. Dots represent individual patients. Two-sided Wilcoxon test, unless otherwise specified. * $P < 0.05$, ** $P < 0.01$, *** $P < 0.001$.

were highest during acute COVID-19 and remained elevated over time (Fig. 3C). ELISA measurements of sC5b-9 complexes, detecting a neoepitope of the fully assembled TCC, showed increasing concentrations with acute COVID-19 severity, but no differences at 6-month follow-up (Fig. 3D). Long Covid patients who recovered before 6-month follow-up and 6-month

Long Covid patients had elevated sC5b-9 levels during the initial acute COVID-19 phase, whereas sC5b-9 levels were unchanged at 6-month follow-up (Fig. 3E and fig. S3B). In contrast, complement activity, determined by a CH50 equivalent assay measuring total sC5b-9 formation upon in vitro complement activation, revealed increased lytic activity,

both during acute COVID-19 and at 6-month follow-up, in 6-month Long Covid patients but not in recovered Long Covid patients (Fig. 3, F and G, and fig. S3C).

To determine which TCC components were associated with increased sC5b-9 formation upon complement activation, we applied statistical modeling (linear mixed-effects model),

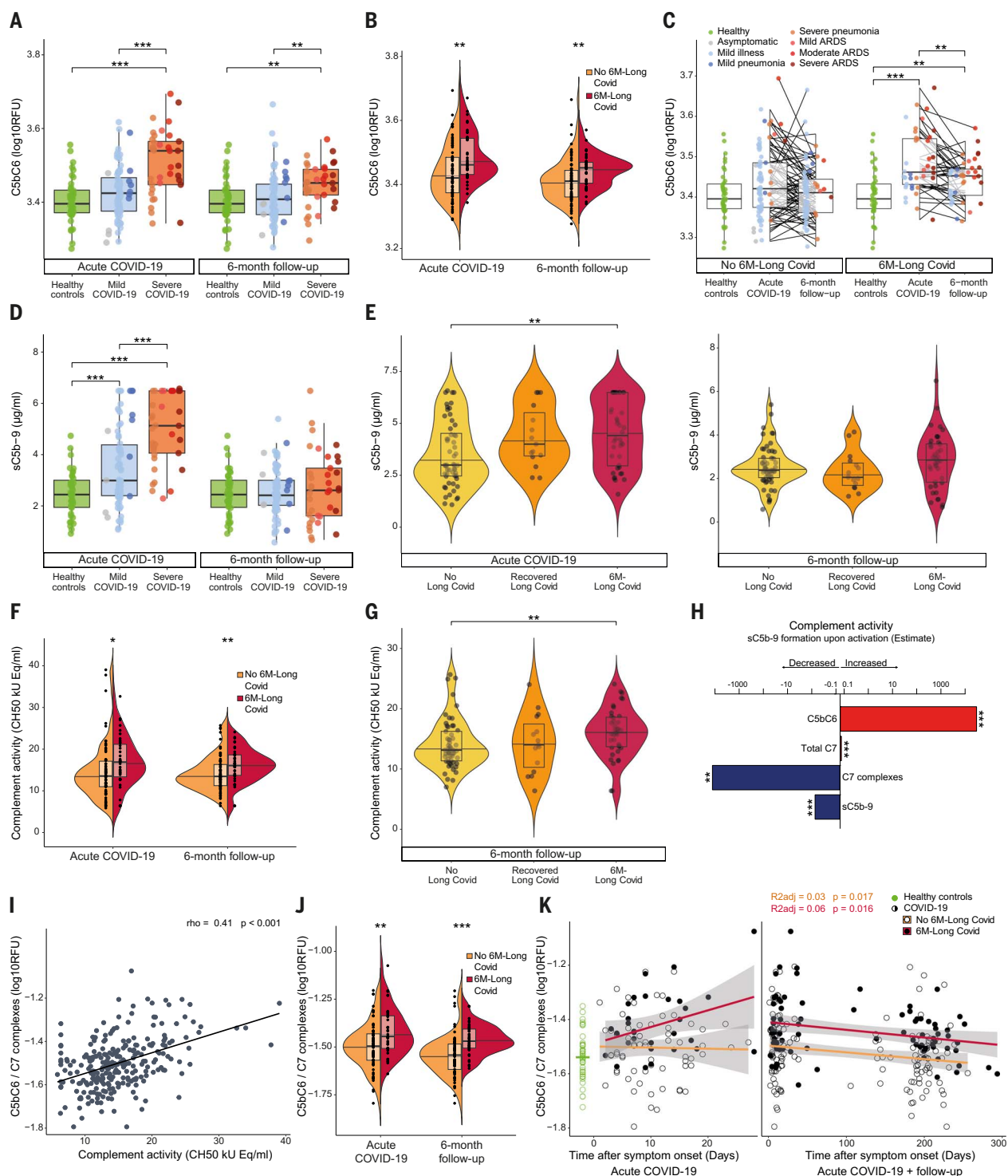


Fig. 3. Increased complement activity in Long Covid. (A) Complement C5bC6 complex (C5bC6) in healthy controls and mild and severe COVID-19 patients, at acute COVID-19 and 6-month follow-up. (B and C) C5bC6 in patients without or with 6-month Long Covid, at acute COVID-19 and 6-month follow-up (B), (paired test) compared to healthy controls (C). Lines connect corresponding patients. (D and E) Soluble C5b-9 (sC5b-9; ELISA) in healthy controls and mild or severe COVID-19 patients (D), and patients with no Long Covid, recovered Long Covid, or 6-month Long Covid (E), at acute COVID-19 and 6-month follow-up. (F and G) Complement activity (CH50) in patients without or with 6-month Long Covid (F) and patients with no Long Covid, recovered Long Covid (G). (H) Complement activity upon activation (Estimate). (I) Spearman correlation of C5bC6/C7 complex ratio and complement activity. (J) C5bC6/C7 complex ratio in patients without or with 6-month Long Covid, at acute COVID-19 and 6-month follow-up. (K) C5bC6/C7 complex ratio in patients without or with 6-month Long Covid, relative to time, with linear models. Healthy controls with median (left). Dots represent individual patients. Two-sided Wilcoxon test, unless specified otherwise. * $P < 0.05$, ** $P < 0.01$, *** $P < 0.001$.

or 6-month Long Covid (G), at acute COVID-19 and 6-month follow-up. (H) Linear mixed-effects model of complement activity as a function of complement levels, adjusted for age, sex, severe COVID-19, 6-month Long Covid, and sampling time point, using acute COVID-19 and 6-month follow-up data. (I) Spearman correlation of C5bC6/C7 complex ratio and complement activity. (J) C5bC6/C7 complex ratio in patients without or with 6-month Long Covid, at acute COVID-19 and 6-month follow-up. (K) C5bC6/C7 complex ratio in patients without or with 6-month Long Covid, relative to time, with linear models. Healthy controls with median (left). Dots represent individual patients. Two-sided Wilcoxon test, unless specified otherwise. * $P < 0.05$, ** $P < 0.01$, *** $P < 0.001$.

considering patient age, sex, COVID-19 severity, 6-month Long Covid status, and sampling time point (Fig. 3H and fig. S3D). Combining acute COVID-19 and 6-month follow-up data, we found increased complement activity in COVID-19 patients to be associated with high levels of early TCC components, including C5bC6 and total C7, as well as low levels of late TCC formations, including C7 complexes and sC5b-9 (Fig. 3H). As C5bC6 and C7 complexes showed a negative correlation (fig. S3E), we calculated the C5bC6/C7 complex ratio, which strongly correlated with complement activity in study participants (Fig. 3I). The C5bC6/C7 complex ratio was increased in 6-month Long Covid patients, both during acute COVID-19 and 6 months later (Fig. 3J), with a tendency toward higher levels during acute COVID-19, followed by a gradual decrease with time (Fig. 3K), which was not influenced by patient age (fig. S3F). C7 complexes and the C5bC6/C7 complex ratio were similarly reduced at 6-month follow-up in all patients with 6-month Long Covid, regardless of whether they progressed to 12-month Long Covid (fig. S3G) and independent of frequency or quality of Long Covid symptoms (fig. S3, H to K). Collectively, increased complement activity in Long Covid patients at 6-month follow-up was marked by elevated early TCC formations, whereas reduced late TCC formations suggested membrane insertion of TCCs.

Association of classical and alternative complement activation with Long Covid

The classical and lectin complement activation pathways converge in activation of complement C2 and C4, followed by conversion of C3 to active C3b, thus initiating the assembly of C5 convertase, which results in TCC formation (27). Factor B is a central component of the alternative pathway. Moreover, C5 can be activated directly by thrombin by cross-talk with the blood coagulation system and initiate TCC formation (33, 34) (Fig. 4A). We therefore investigated whether changes to the upstream complement activation pathways were associated with Long Covid. We detected increased C2 levels in 6-month Long Covid patients during acute COVID-19 and at 6-month follow-up (Fig. 4B), indicating classical or lectin pathway activation. ELISA measurement of the C4 cleavage product, C4d, revealed transiently increased C4d during acute COVID-19 but no differences based on Long Covid history (Fig. 4C and fig. S4A). Conversely, mannose-binding lectin (MBL), a central component of the lectin pathway, was unaltered between patients with and without 6-month Long Covid at 6-month follow-up (fig. S4B).

During acute COVID-19, factor B levels were increased in 6-month Long Covid patients compared with patients without Long Covid and healthy controls (Fig. 4D and fig. S4C).

ELISA measurement of the cleavage product, factor Ba, confirmed increased levels in Long Covid patients during acute COVID-19 (fig. S4, C and D). At 6-month follow-up, factor Ba levels were persistently elevated in 6-month Long Covid patients compared with patients without Long Covid and healthy controls (Fig. 4E and fig. S4E). Complement C3d, the final degradation product of C3, was also elevated in 6-month Long Covid patients at 6-month follow-up compared with healthy controls (Fig. 4F). We analyzed serum levels of the thrombin inhibitor antithrombin III and found persistently low levels in 6-month Long Covid patients during acute COVID-19 and at 6-month follow-up (Fig. 4G and fig. S4E). In a subset of the Mount Sinai cohort ($n = 21$), we consistently found increased complement C3d and decreased antithrombin III in 6-month Long Covid patients at 3-month follow-up compared with patients without 6-month Long Covid, patients hospitalized for reasons unrelated to COVID-19, and healthy controls (Fig. 4H; fig. S4, F and G; and table S3).

To validate complement system dysregulation further, we performed mass spectrometry on 6-month follow-up serum samples of COVID-19 patients in our cohort. Complement components were among the top differentially abundant proteins in 6-month Long Covid patients compared with patients without 6-month Long Covid (Fig. 4I). Consistent with our previous analyses, complement C5 and factor B were increased and antithrombin III was decreased in 6-month Long Covid patients (Fig. 4J). In 6-month Long Covid patients, C5 was the only TCC component with significantly altered total levels (fig. S4H). Analysis of additional complement components showed increased complement regulatory proteins factor I, factor H, and C4-binding protein beta (C4BPB) and confirmed increased C2 in 6-month Long Covid patients (Fig. 4K). Interestingly, C2 was most elevated in 6-month Long Covid patients experiencing fatigue (fig. S4I) and 6-month Long Covid patients progressing to 12-month Long Covid (Fig. 4L) but showed no significant association with the number of 6-month Long Covid symptoms (fig. S4J). Instead, C2 highly correlated with C4BPB serum levels (fig. S4J), thus possibly explaining the high C2 levels in the presence of normal C4d levels. C2 levels measured by mass spectrometry at 6-month follow-up distinguished between patients developing 12-month Long Covid and those recovering before 12-month follow-up, as quantified by an area under the curve (AUC) of 0.81 (Fig. 4M). Other proteins of the complement system, such as C3 desArg, C5a, clusterin, vitronectin, and the pentraxins CRP, pentraxin 3 (PTX3), and serum amyloid A4 measured by SomaScan, mass spectrometry, or ELISA were unchanged (fig. S4K).

Analysis of antithrombin III peptides by mass spectrometry showed a decrease of peptide intensities after the reactive site with thrombin in 6-month Long Covid patients (fig. S4L). The ratio of peptide intensities on either side of this cleavage site was increased in 6-month Long Covid patients (Fig. 4N), suggesting increased cleavage of antithrombin III (35). Peptides at a heparin-binding region of antithrombin III were also decreased, accompanied by a decrease of the potential binding partner heparan sulfate proteoglycan 2 (HSPG2; fig. S4, L and M) (35–37). Analysis of other components of the coagulation system showed increased coagulation factor XI, fibrinogen beta, protein C, and heparin cofactor II in 6-month Long Covid patients (Fig. 4O). Altogether we demonstrated, by two approaches, classical and alternative complement system activation as well as low antithrombin III levels and increased cleavage of antithrombin III at the thrombin-reactive site.

Signs of complement-mediated tissue injury in Long Covid

Downstream effects of pathological complement activation entail hemolysis; induction of thromboinflammatory responses, including platelet and endothelial activation; and changes in innate immune cells, such as neutrophils (38–40). Combining SomaScan and mass spectrometry proteomics, we assessed a total of 84 measurements of 49 different serum biomarkers in the above-mentioned cell types (data S5) (41–46). Statistical modeling identified eight measurements associated with 6-month Long Covid, including decreased hemopexin (three times), ICAM-1, and S100-A8/A9, as well as increased thrombospondin-1 (TSP-1; twice) and von Willebrand factor (vWF) (Fig. 5A). ICAM-1 levels were persistently low during acute COVID-19 and at 6-month follow-up in 6-month Long Covid, suggesting low baseline levels (fig. S5A). Low levels of hemopexin, a marker of increased heme levels, were accompanied by normal hemoglobin and myoglobin levels (Fig. 5B and fig. S5B). An additional colorimetric assay was performed on 6-month follow-up samples of COVID-19 patients to quantify heme in serum, which revealed an association of increased heme with 6-month Long Covid and confirmed correlation of decreased hemopexin with increased heme (Fig. 5C and fig. S5C). Erythrocyte counts were unchanged, whereas haptoglobin was increased in 6-month Long Covid patients, along with slightly elevated interleukin-6 (IL-6) levels (Fig. 5B and fig. S5B). Measurements of transferrin, a marker of iron homeostasis, revealed a tendency toward reduced levels in 6-month Long Covid patients at 6-month follow-up (fig. S5B). Other markers of hemolysis and muscle cell injury as well as neutrophil and thrombocyte counts were unchanged overall (Fig. 5D and fig. S5, D and E).

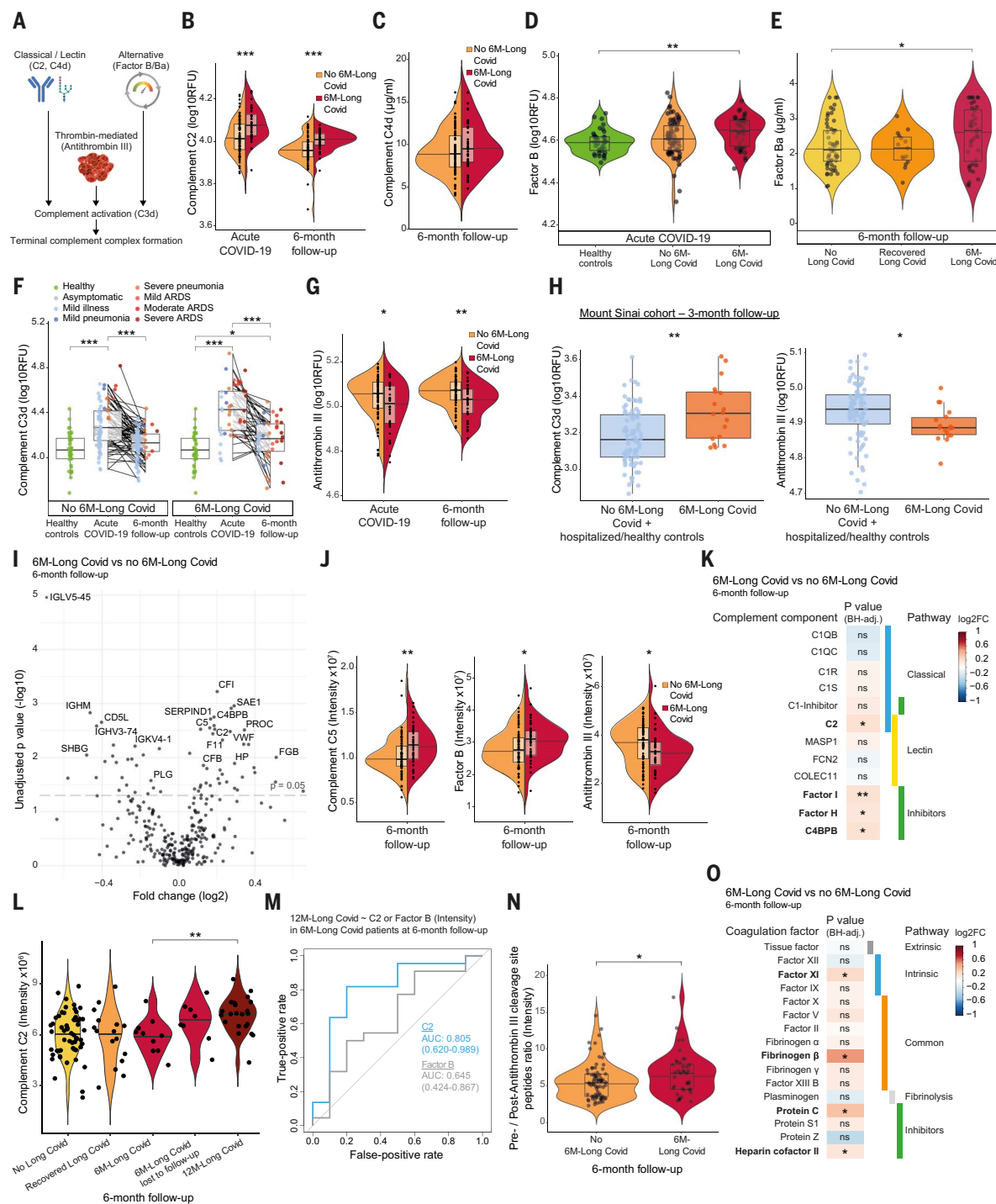


Fig. 4. Complement activation pathways at 6-month follow-up. (A) Schematic of pathways. [Created with BioRender.com] (B and C) C2 (B) and C4d (C) in patients without or with 6-month Long Covid, at acute COVID-19 or 6-month follow-up. (D) Factor B in healthy controls, patients without or with 6-month Long Covid, at acute COVID-19. (E) Factor Ba (ELISA) in patients with no Long Covid, recovered Long Covid, or 6-month Long Covid, at 6-month follow-up. (F) C3d in patients without or with 6-month Long Covid, at acute COVID-19 and 6-month follow-up (paired test), compared with healthy controls. Lines connect corresponding patients. (G) Antithrombin III in patients without or with 6-month Long Covid, at acute COVID-19 and 6-month follow-up. (H) C3d and antithrombin III in healthy and patient controls (blue; $n = 85$), and 6-month Long Covid patients (red; $n = 18$) of Mount Sinai cohort at 3-month follow-up. (I) Differential proteins (mass spectrometry) in patients with versus without 6-month Long Covid. (J) C5, factor B, and antithrombin III in patients without or with 6-month Long Covid, at 6-month follow-up. (K) Differential complement proteins (BH-adjusted) in patients with versus without 6-month Long Covid, at 6-month follow-up. (L) C2 in patients with no Long Covid, recovered Long Covid, 6-month Long Covid, 6-month Long Covid lost to follow-up, or 12-month Long Covid, at 6-month follow-up. (M) Area under the curve (AUC) for prediction of 12-month Long Covid as a function of C2 or factor B, in 6-month Long Covid patients at 6-month follow-up, using logistic regression. (N) Ratio of antithrombin III peptides intensity before and after thrombin-reactive site, in patients without or with 6-month Long Covid, at 6-month follow-up. (O) Differential coagulation proteins in patients with versus without 6-month Long Covid, at 6-month follow-up. Dots represent individual patients. Two-sided Wilcoxon test, unless specified otherwise. ns, nonsignificant; * $P < 0.05$, ** $P < 0.01$, *** $P < 0.001$.

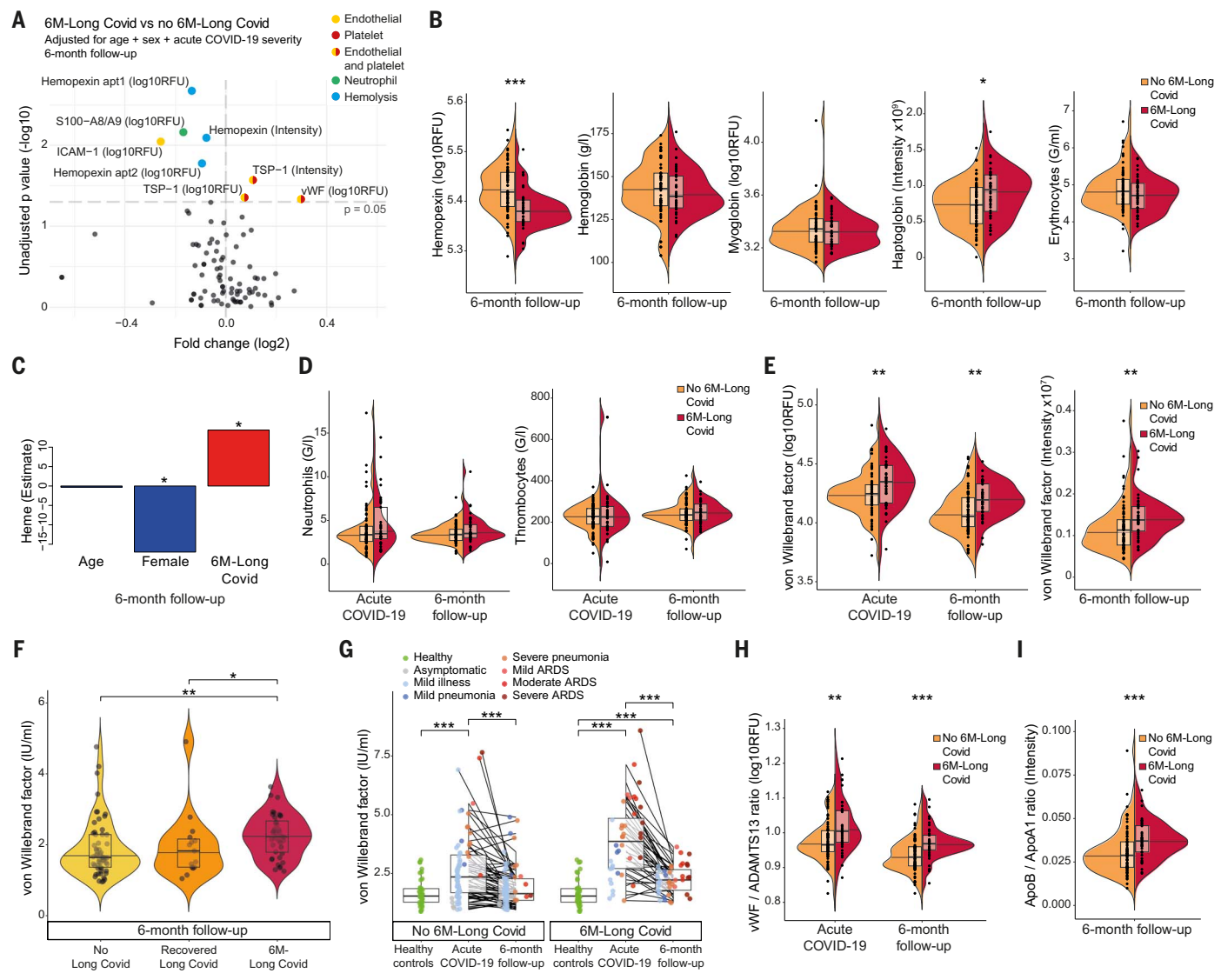


Fig. 5. Tissue injury markers in Long Covid. (A) Differential proteins [SomaScan aptamers (apt) and mass spectrometry; logistic regression] in patients with versus without 6-month Long Covid, at 6-month follow-up, including 84 measurements of 49 tissue injury markers (data S5). (B) Hemopexin, hemoglobin, myoglobin, haptoglobin, and erythrocyte counts in patients without or with 6-month Long Covid, at 6-month follow-up. (C) Linear model of heme (colorimetric assay) as a function of patient age, sex, and 6-month Long Covid, in COVID-19 patients at 6-month follow-up. (D) Neutrophil and thrombocyte counts in patients without or with 6-month Long Covid, at acute COVID-19 and 6-month follow-up. (E) Von Willebrand factor [vWF; SomaScan (left) and mass

spectrometry (right)] in patients without or with 6-month Long Covid, at acute COVID-19 and 6-month follow-up. (F) vWF (ELISA) in patients with no Long Covid, recovered Long Covid, and 6-month Long Covid, at 6-month follow-up. (G) vWF in patients without or with 6-month Long Covid, at acute COVID-19 and 6-month follow-up (paired test), compared with healthy controls. Lines connect corresponding patients. (H and I) vWF/ADAMTS13 ratio (H) or ApoB/ApoA1 ratio [mass spectrometry; (I)] in patients without or with 6-month Long Covid, at acute COVID-19 or 6-month follow-up. Dots represent individual patients. Two-sided Wilcoxon test, unless specified otherwise. * $P < 0.05$, ** $P < 0.01$, *** $P < 0.001$.

Serum levels of vWF, measured by SomaScan, mass spectrometry, and an ELISA calibrated to WHO standards, were increased in 6-month Long Covid patients both during acute COVID-19 and at 6-month follow-up but not in recovered Long Covid patients (Fig. 5, E to G, and fig. S5, F and G). The regulatory counterpart of vWF, ADAMTS13 (47), was decreased in 6-month Long Covid patients at 6-month follow-up (fig. S5H). The vWF/ADAMTS13 ratio, a marker of thromboinflammation and endothelial dysreg-

ulation (45, 47, 48), was increased in 6-month Long Covid patients both during acute COVID-19 and at 6-month follow-up (Fig. 5H). Both, vWF and the vWF/ADAMTS13 ratio showed positive correlation with complement activity (fig. S5I). Notably, at 6-month follow-up, vWF levels were lower in hospitalized patients who had received antiviral treatment with remdesivir during acute COVID-19 when compared with hospitalized patients who had not been treated with remdesivir (fig. S5J). Moreover,

we detected increased coagulation factor VIII (FVIII) levels in 6-month Long Covid patients at 6-month follow-up (fig. S5K), which could be explained by vWF acting as a carrier of FVIII. In line with this thromboinflammatory signature, we also observed decreased platelet-activating factor acetylhydrolase (PAF-AH) and an increased ratio of low-density lipoprotein component apolipoprotein B (ApoB) to high-density lipoprotein component ApoA1 in 6-month Long Covid patients (Fig. 5I and fig. S5L), which is

an established cardiovascular risk factor (49). Antithrombin III and vWF levels were not affected by the presence of fatigue (fig. S5M). Collectively, Long Covid was characterized by elevated tissue injury markers, such as hemolysis and endothelial and platelet activation.

Increased monocyte–platelet aggregates in Long Covid patients

Next, we explored thromboinflammatory signatures on a cellular level. We performed spectral flow cytometry on peripheral blood mononuclear cells (PBMCs) from seven healthy controls, five COVID-19 patients without 6-month Long Covid, and ten 6-month Long Covid patients, of whom six progressed to 12-month Long Covid, all sampled at 6-month follow-up (Fig. 6A). These analyses were paired with single-cell transcriptomics of flow cytometry-sorted monocytes. Comparing cellular markers in these four groups, we found different phenotypes in cell clusters corresponding to classical monocytes (Fig. 6, B to D, and fig. S6A). We also measured CD41, a platelet marker usually absent on monocytes; thus, CD41-positive monocytes correspond to aggregates of monocytes with platelets (50). Based on CD41 surface abundance, classical monocytes were further manually subclustered into CD41^{high}, CD41^{dim}, and CD41^{neg} monocytes (Fig. 6E). Frequencies of CD41^{high} monocytes were highest in 12-month Long Covid patients (Fig. 6, B and F).

Flow cytometry-sorted monocytes of healthy controls were negative for CD41; however, adding platelets to these monocytes increased their CD41 abundance, regardless of activation by lipopolysaccharide (Fig. 6G and fig. S6, B to D), demonstrating that CD41^{high} monocytes represented monocyte–platelet aggregates. On direct ex vivo analysis of cells, CD41 surface expression on monocytes was lowest in healthy controls and highest in Long Covid patients (Fig. 6H). Notably, CD41^{high} monocytes showed different marker expression profiles than CD41^{dim} and CD41^{neg} monocytes, including increased CD55, also known as complement decay-accelerating factor (Fig. 6I). Single-cell transcriptomics of sorted monocytes (Fig. 6J) did not reveal a prothrombotic transcriptional signature of monocytes (Fig. 6K) but did confirm their absent *Cd41* mRNA expression (fig. S6E). We found low abundance of *IL1B* and *NR4A1*, particularly in classical monocytes, and increased expression of the interferon-induced transmembrane protein *IFITM3* (Fig. 6K and fig. S6, F to H). Altogether, we found monocyte–platelet aggregates in Long Covid patients at 6-month follow-up, which were highest in patients progressing to 12-month Long Covid.

Association of classical complement activation with IgG against herpesviruses

To identify antibodies potentially driving classical complement activation in 6-month Long

Covid patients, we investigated autoantibodies and antiviral antibodies. Using a highly sensitive indirect immunofluorescence assay, we assessed antinuclear antibody (ANA) titers at 6-month follow-up and detected an increased prevalence of ANA positivity in 6-month Long Covid patients compared with patients without 6-month Long Covid (fig. S7A). ANA fluorescence patterns were mainly of nonspecific or fine speckled fluorescence across the nucleoplasm in 6-month Long Covid patients, whereas in ANA-positive patients without 6-month Long Covid, nucleolar patterns were more frequent (fig. S7B), which suggests different autoantibody specificities. Anti-chemokine antibodies, previously described to be protective in Long Covid, were measured in a subset of 88 COVID-19 patients. Statistical modeling revealed low anti-CXCL13 to be significantly associated with 6-month Long Covid (fig. S7, C and D), confirming published data (51).

High-throughput measurement of antiviral antibodies was performed by phage immunoprecipitation sequencing technology (VirScan) for a total of 87,890 epitopes in a subset of 57 COVID-19 patients during acute disease, including 22 that developed 6-month Long Covid, and 18 healthy controls (Fig. 7A and table S5). Although we found no overall increase in reactivity to viral epitopes in 6-month Long Covid patients compared with patients without 6-month Long Covid and healthy controls, IgG titers against herpesviruses 1 to 8 were increased proportionally (Fig. 7, A and B). On the epitope level, we observed low IgG against enterovirus B and high IgG against human herpesvirus 5 [also known as cytomegalovirus (CMV)] in 6-month Long Covid patients (Fig. 7, C and D). Statistical models showed associations of low anti-enterovirus IgG with patient age and of high anti-CMV IgG with 6-month Long Covid (fig. S7E).

On the basis of these data and previous reports on Epstein-Barr virus (EBV) reactivation (52), we measured serum titers of IgM and IgG against CMV and EBV at 6-month follow-up. Whereas antiviral IgM is increased during active viral replication, antiviral IgG indicates an immune response to past infection (53). Overall serum positivity for CMV- and EBV-specific IgG and, thus, prevalence of CMV or EBV infection did not differ between patients with and patients without 6-month Long Covid (Fig. 7E). We also found no difference in anti-CMV and anti-EBV IgM titers (Fig. 7F and fig. S7F). However, both anti-CMV and anti-EBV IgG were increased in 6-month Long Covid patients (Fig. 7F and fig. S7F). Statistical modeling confirmed the association of high anti-CMV and anti-EBV IgG titers with 6-month Long Covid (Fig. 7G). Notably, C2 levels were associated with anti-CMV IgG titers and 12-month Long Covid (Fig. 7H). We found no differences in serum IgG antibodies targeting four differ-

ent SARS-CoV-2 spike epitopes in patients with and patients without 6-month Long Covid (Fig. 7I and fig. S7G) and no evidence of SARS-CoV-2 or herpesviral transcripts in monocytes (Fig. 7J). Analysis of previously reported inflammatory markers in Long Covid showed that interferon alpha 2 inversely correlated with C7 complexes, and IL-6 correlated with C5bC6 complexes in COVID-19 patients at 6-month follow-up (fig. S7H). Altogether, increased titers of antibodies against herpesviruses in Long Covid patients were associated with C2 of the classical complement pathway, suggesting that viral antigen–antibody immune complexes could be involved in activation of this pathway.

Serum proteomics for Long Covid diagnosis and prediction

To translate the observed differences into a predictive model for 6-month Long Covid, we included up to 61 uncorrelated protein epitope measurements of involved biological pathways (with absolute Spearman correlation coefficients below 0.3), two protein ratios, and information on medical history (14 variables) (data S8). For diagnostic purposes, we included only protein measurements and medical history obtained at 6-month follow-up to identify diagnostic biomarkers associated with 6-month Long Covid and, thus, normal in recovered patients and healthy controls. We applied a random forest classifier, a machine learning algorithm suitable for analyzing large datasets. Through iterative assessment of acute COVID-19 and 6-month follow-up data, the algorithm identified the most influential biomarkers for predicting Long Covid. The models were trained through fivefold nested cross-validation, with model hyperparameters being tuned on the training part of the data (Fig. 8A). Relevant data splits were stratified for acute COVID-19 severity. The resulting predictions performed well in the unseen test sets (corresponding to patient data not used for training the prediction model), as quantified by the area under the receiver operator characteristic (AUROC; $\geq 0.74 \pm 0.10$ for 6-month Long Covid) and relative average precision scores accounting for Long Covid prevalence and class imbalance (Fig. 8B and fig. S8A).

Studying the intricate interplay of features driving the prediction, we identified patient age, C5bC6/C7 complex ratio, vWF/ADAMTS13 ratio, and patient body mass index (BMI) as the driving variables (Fig. 8C). These four variables were sufficient to predict 12-month Long Covid (mean AUC of 0.81 ± 0.08) in a cohort of both healthy and COVID-19 subjects. Addition of the two protein ratios to age and BMI improved model performance in all scenarios (Fig. 8B and fig. S8, A and B). Inclusion of healthy controls in the group not developing Long Covid reduced the association of Long Covid with potentially preexisting risk factors

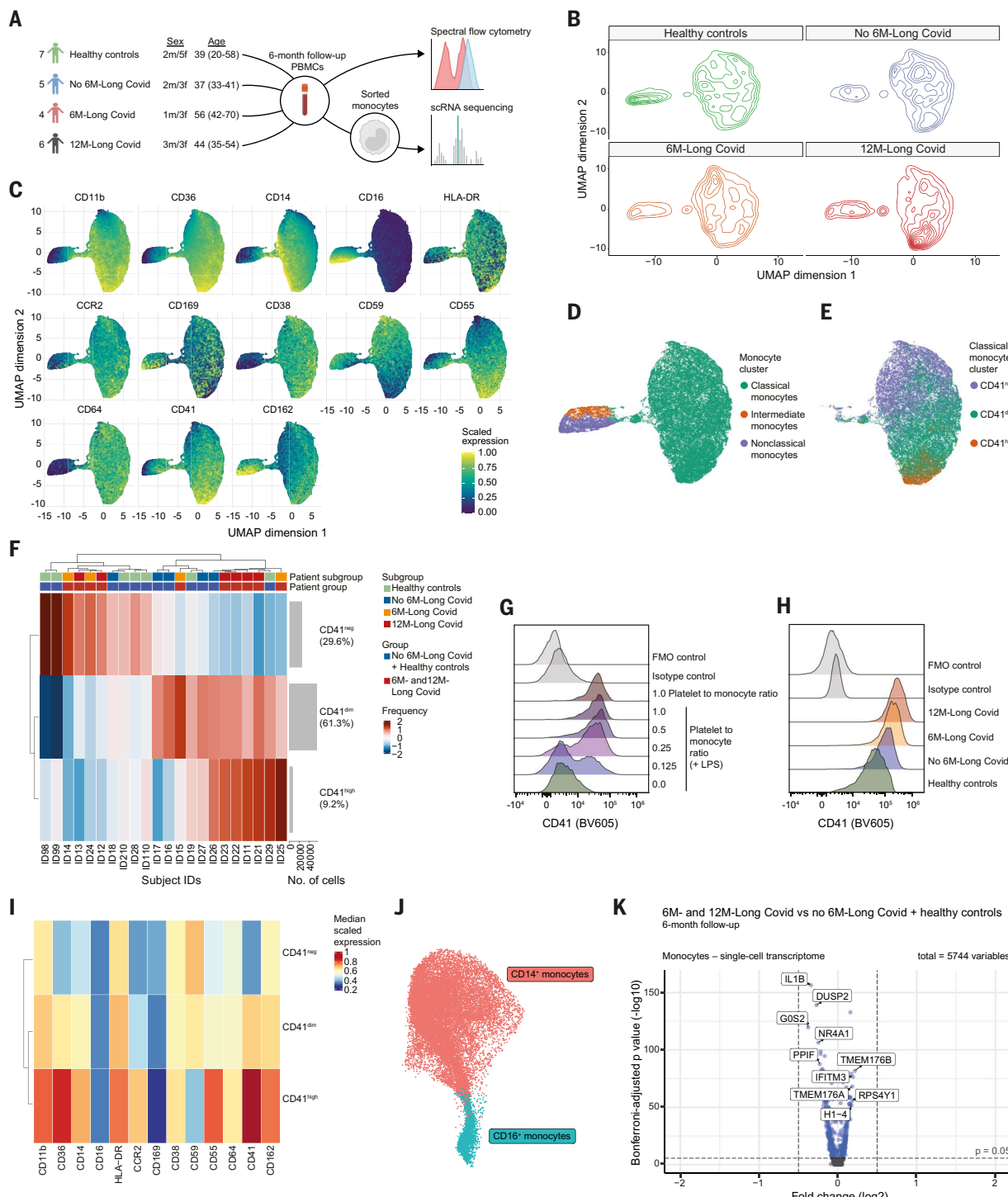


Fig. 6. Increased monocyte-platelet aggregates in Long Covid. **(A)** Overview of groups for spectral flow cytometry and sorting of PBMCs isolated at 6-month follow-up, for single-cell RNA (scRNA) sequencing of monocytes. Six-month Long Covid patients were subgrouped into patients with or without recovery before 12-month follow-up. For scRNA sequencing, five out of seven healthy controls were analyzed [sex: 1m/4f; age: 44 (23–65)]. A total of 19,247 monocytes were sequenced. [Created with [BioRender.com](#)] **(B)** Uniform manifold approximation and projection (UMAP) density plots of gated monocytes (spectral flow cytometry) of indicated groups. **(C)** UMAPs of scaled marker expression of monocytes. **(D and E)** UMAPs of all (D) and classical monocytes manually subclustered on the basis of CD41 expression profiles (E). **(F)** Relative (inside heatmap) and cumulative (gray bars)

abundance of classical monocytes subclustered on the basis of CD41 expression, in indicated individual donors. Frequencies of CD41-subclustered classical monocytes indicate Z-score-normalized proportion of subclusters within total classical monocytes. **(G)** CD41 surface abundance on sorted monocytes incubated with indicated ratios of platelets, without or with lipopolysaccharide (LPS) prestimulation. **(H)** CD41 surface abundance on classical monocytes from indicated groups. **(I)** Scaled marker expression in CD41-subclustered classical monocytes. **(J)** UMAP of all monocytes (scRNA sequencing). **(K)** Volcano plot of differentially expressed RNA transcripts in monocytes of Long Covid patients (6- and 12-month Long Covid) versus controls (no 6-month Long Covid and healthy controls), at 6-month follow-up. Vertical dashed lines indicate \log_2 fold change of -0.5 and 0.5.

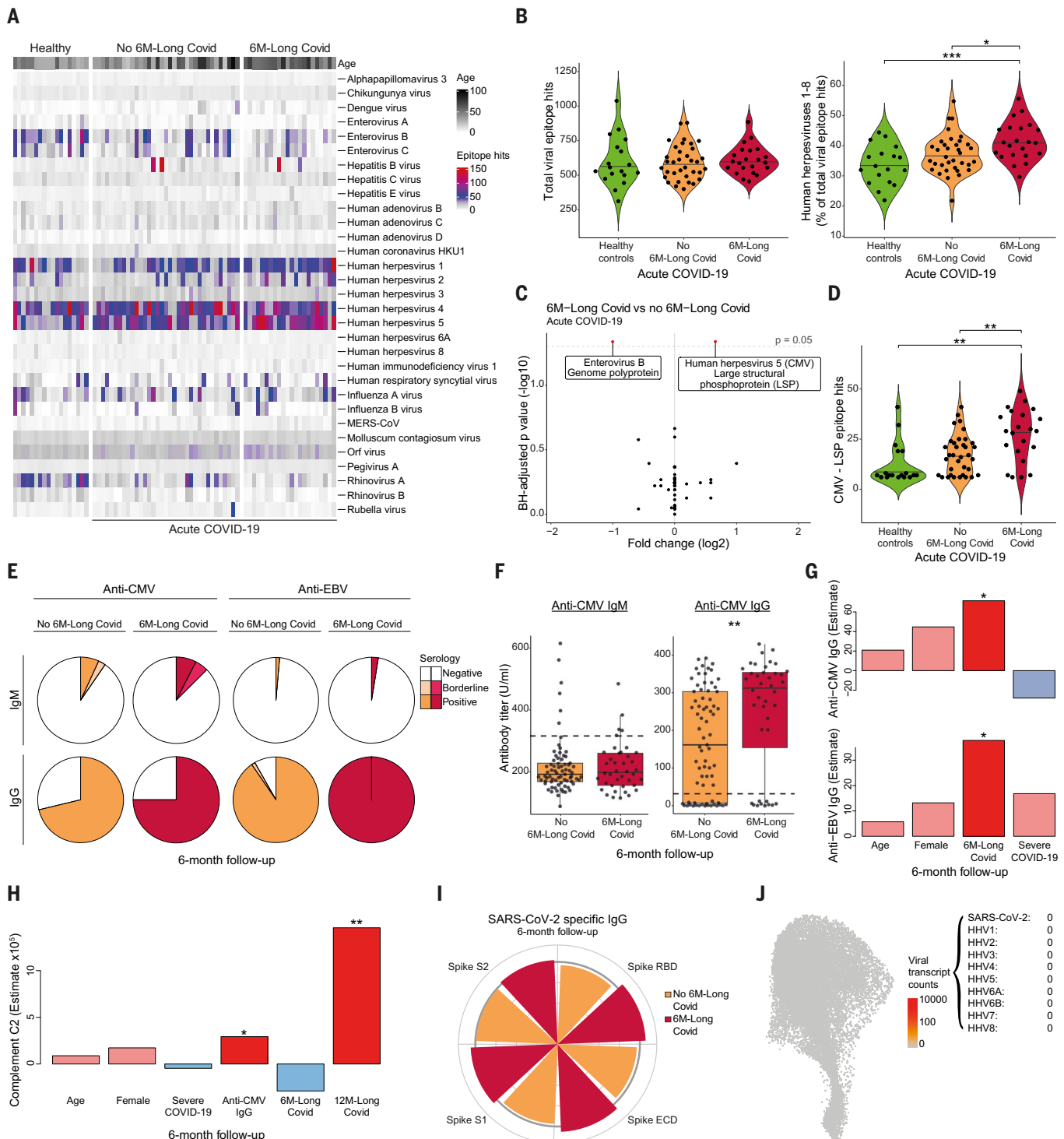


Fig. 7. Increased antibody reactivity against herpesviruses in Long Covid.
(A) Antiviral IgGs (VirScan) in healthy controls ($n = 18$) and patients without ($n = 35$) or with 6-month Long Covid ($n = 22$), during acute COVID-19. Viruses with >300 epitope hits. **(B)** Total viral (left) and percentage of herpesviral (right) epitope hits in healthy controls and patients without or with 6-month Long Covid, with median. **(C)** Differential abundance of viral epitope-specific IgG in patients with versus without 6-month Long Covid, BH-adjusted. **(D)** CMV LSP epitope hits in healthy controls and patients without or with 6-month Long Covid. **(E)** Serum reactivity for anti-CMV (left) and anti-EBV (right), and IgM (top) and IgG (bottom) in patients without (orange) or with (red)

6-month Long Covid, at 6-month follow-up (ELISA; $n = 113$). **(F)** Anti-CMV IgM (left) and IgG (right) in patients without or with 6-month Long Covid. **(G and H)** Linear model coefficients for anti-CMV or anti-EBV IgG titers (G) and C2 (H). **(I)** Radar plot. Wedge sizes represent median IgG titers of patients without or with 6-month Long Covid, normalized to median titers of all patients, at 6-month follow-up. **(J)** UMAP of monocytes showing absence of intracellular herpesviral and SARS-CoV-2 transcripts (scRNA sequencing). ECD, extracellular domain; RBD, receptor binding domain. Dots represent individual patients. Two-sided Wilcoxon test, unless specified otherwise.

* $P < 0.05$, ** $P < 0.01$, *** $P < 0.001$.

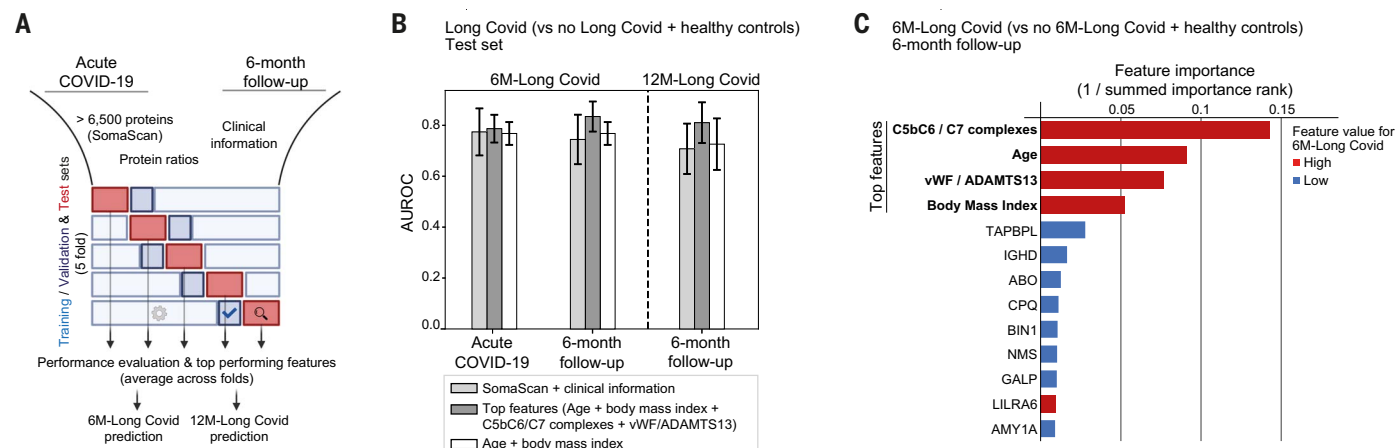


Fig. 8. Predictive and diagnostic models of Long Covid. (A) Overview of model training strategy by nested cross-validation. For each fold, models were trained on training portion of data with hyperparameters adjusted on the basis of validation set. Each trained model was evaluated on an unseen test set. [Created with BioRender.com] (B) Area under the receiver operating characteristics curve (AUROC) of a random forest predictor using up to 61 uncorrelated protein measurements, 2 protein ratios, 14 general clinical variables, top selected features of 6-month Long Covid prediction selected on training data [age, body mass index (BMI), C5bC6/C7 complexes, and vWF/ADAMTS13 ratio], or age and BMI alone.

Input measurements obtained at acute COVID-19 or 6-month follow-up for prediction of 6-month Long Covid versus no 6-month Long Covid and healthy controls ($n = 40, 73$, and 39 , respectively), and at 6-month follow-up for prediction of 12-month Long Covid versus no 12-month Long Covid and healthy controls ($n = 22, 73$, and 39 , respectively; mean \pm SD). (C) Top features of prediction of 6-month Long Covid versus no 6-month Long Covid and healthy controls, using 6-month follow-up measurements. Summed importance rank was calculated over all five cross-validation folds. Top selected features were identified by elbow analysis.

in healthy controls, thus increasing specificity of identified biomarkers for active Long Covid. We also tested the models upon exclusion of healthy controls and consistently confirmed the diagnostic and predictive potential of the protein biomarkers (fig. S8C). Collectively, machine learning algorithms independently identified complement and thromboinflammatory markers as top protein biomarkers of active Long Covid.

Discussion

New SARS-CoV-2 variants have confronted the world with repeated SARS-CoV-2 infection (54), contributing to a high prevalence of Long Covid (55). We identified common patterns in the serum proteome of Long Covid patients not recovered at 6 months after acute infection by studying a prospective cohort of mild and severe COVID-19 patients and healthy controls.

Analysis of >7000 protein measurements revealed the complement system as the top dysregulated biological pathway in Long Covid. At 6-month follow-up, late TCC formations, comprising the soluble C7 complexes C5b-7, C5b-8, and C5b-9, were reduced in individuals experiencing active Long Covid. These findings were paralleled by an increase of the early TCC formation C5bC6 and increased complement activity. The imbalance in TCC formations was best quantified by a C5bC6/C7 complex ratio, also identified by machine learning as the top predictive biomarker of Long Covid. Binding of C7 to the stable bimolecular complex C5bC6 enables the trimolecular C5b-7

complex to integrate into cell membranes (30). Our observation of increased complement activity in the presence of elevated C5bC6 levels and decreased soluble C7 complexes suggested increased membrane insertion of TCCs in active Long Covid.

Increased factor Ba levels suggested alternative complement pathway activation as a possible driver of TCC formation (27). Moreover, increased C2, reflecting classical complement pathway activation, was associated with Long Covid persistence. Our finding of increased anti-CMV and anti-EBV IgG titers in Long Covid patients at 6-month follow-up suggested increased viral antigen exposure and, thus, antiviral antibody formation in Long Covid patients, perhaps through reactivation of herpesviruses. The association of C2 levels with anti-CMV IgG titers and Long Covid persistence may connect our finding of increased complement activation to recent reports of herpesvirus reactivation in Long Covid (52). Furthermore, C5 could be activated directly through thrombin, as supported by our findings of a dysregulated coagulation cascade, low antithrombin III levels in Long Covid patients in two independent cohorts, and increased antithrombin III cleavage at the thrombin-reactive site (33–36).

Elevated vWF and TSP-1 along with decreased protective factors, such as ADAMTS13, PAF-AH, and ApoAI, indicated thromboinflammatory responses, which can also drive complement activation (38, 39, 47). Both vWF and TSP-1 can be secreted by endothelial cells and thrombocytes. Persistently low ICAM-1

levels in Long Covid patients argue against strong endothelial activation and have been associated with genetic ICAM-1 variants (41, 56). The finding of increased monocyte–platelet aggregates in Long Covid patients suggested platelet activation at 6-month follow-up (57). However, normal platelet counts despite the presence of increased monocyte–platelet aggregates indicated compensatory mechanisms. As single-cell monocyte transcriptomes lacked signs of a prothrombotic signature, aggregates may be driven by platelet activation rather than by monocytes (50). However, monocytes showed distinct transcriptomic changes in Long Covid patients, including decreased NR4A1 and increased transcripts for interferon-induced transmembrane proteins. Interestingly, NR4A1-dependent monocyte subsets have been associated with endothelial homeostasis in mice (58). Moreover, increased interferon-induced transcripts have been associated with severe cases of SARS-CoV-2 infection (59). As with monocytes, we did not observe any increased markers of neutrophil activation and NETosis, and neutrophil counts were normal at 6-month follow-up.

Pathological complement activation has been previously associated with thromboinflammatory and microangiopathic manifestations (38). Chronic diseases involving complement activation include neurodegenerative diseases (60) as well as atypical hemolytic uremic syndrome and paroxysmal nocturnal hemoglobinuria, which are marked by complement-mediated hemolysis (38). We found signs of a hemolytic process in Long Covid, including low hemopexin

and increased heme levels in Long Covid patients. Hemopexin–heme complexes are formed upon hemolysis to prevent heme-mediated oxidative damage. These findings were accompanied by increased haptoglobin and IL-6, as well as normal hemoglobin and erythrocyte counts, suggestive of a chronic inflammatory process (42, 61, 62). As tissue injury can be mediated by complement, and in turn also activates the complement system, the observed markers may be both consequence and cause of complement activation. Clinical history and the overall pattern of our findings suggested chronic processes, possibly maintained by external drivers, including chronic herpesvirus infection, or by a self-perpetuating cycle of thromboinflammation.

Excessive complement activation has been reported in severe acute COVID-19 (32). MBL, a central member of the lectin pathway, can directly bind SARS-CoV-2 (63) and is increased in severe pediatric cases (64) but was unchanged at 6-month follow-up in our cohort. Increased PTX3 has been associated with short-term COVID-19 mortality (65) and Long Covid at 8-month follow-up (66) but was not altered in our study by two different methods. Other pathways of complement activation include intracellular mechanisms in SARS-CoV-2-infected host cells (67, 68). COVID-19-associated thromboinflammation has been described in hospitalized patients (32) and has also been proposed to underlie Long Covid (69–71). Brain autopsies of COVID-19 patients showed signs of neurovascular injury accompanied by classical complement component deposition on endothelial cells and platelets (72). Moreover, the vWF/ADAMTS13 ratio was associated with increased thrombogenicity in Long Covid patients (73), and vWF and C7 were among the top enriched proteins in amyloid-like microclots found in Long Covid patients, supporting a central role of C7 (74).

Our multicenter, longitudinal study provides evidence of an inflammatory signature restricted to patients with active Long Covid, with diagnostic accuracy 6 months after symptom onset and independent of any information on COVID-19 history, thus facilitating clinical applicability. Moreover, our findings address the gap between observed complement-activating properties of SARS-CoV-2 and reports of microclots, vascular inflammation, and cardiovascular complications (75). We were able to validate our hypothesis of dysregulated complement activation by different experimental approaches as well as an independent longitudinal cohort of hospitalized COVID-19 patients. However, external validation of our findings with larger cohorts, including Long Covid patients with mild acute COVID-19 and later blood sampling time points, is needed. Larger cohorts might allow more granular assessment of Long Covid subgroups. Other

limitations include caveats of high-throughput biomarker discovery, which were addressed by multiple testing correction, hypothesis-driven analysis, and validation of results by additional methods. The specificity of C7 aptamer for C7 complexes, but not monomeric C7, highlights the need of experimental validations when applying high-throughput approaches.

Given our data, early cardiovascular assessment of Long Covid patients should be considered. Moreover, antivirals targeting SARS-CoV-2 or herpesviruses could reduce thromboinflammatory responses. Available therapeutics targeting the terminal complement pathway could offer new treatment strategies for Long Covid and possibly other postinfection syndromes.

Materials and methods

Experimental study design and Zurich cohort

This study was approved by the Cantonal Ethics Committee of Zurich (BASEC #2016-01440). Adult individuals were included in the study between April 2020 and April 2021 on the basis of RT-qPCR-confirmed SARS-CoV-2 infection. The latest inclusion time point for acute SARS-CoV-2-infected patients was January 2021. Follow-up was continued until 1 year after acute COVID-19 disease, with the last follow-up visit in February 2022.

Following written informed consent, 152 study participants attended one to three study visits (fig. S1A), consisting of a structured questioning by trained physicians and a blood draw. Thirty-nine healthy controls donated blood during the first study visit, and 113 COVID-19 patients donated blood during acute infection as well as 6 months later at the second study visit (6-month follow-up). Eighty-five COVID-19 patients attended a third study visit 12 months after acute COVID-19 (12-month follow-up). Patients unable to attend the 12-month follow-up visit in person were questioned by phone by a trained physician. Eighteen patients declined a 12-month follow-up or could not be contacted. The multicenter study was composed of patients from four different hospitals in the region of Zurich, Switzerland, including the University Hospital Zurich ($n = 77$), City Hospital Triemli ($n = 18$), Limmat Hospital ($n = 13$), and Uster Hospital ($n = 5$). No further inclusion or exclusion criteria were applied on analysis of the 152 study participants. All healthy controls were included at the University Hospital Zurich and reported no history of SARS-CoV-2 infection and no acute or active illness prior to blood sampling, and they had a negative serology for SARS-CoV-2 spike S1-specific IgA and IgG. Participants were mostly Caucasian, and ethnicity was not systematically assessed.

Mount Sinai COVID-19 cohort

This cohort was approved by the Human Research Protection Program at the Icahn School

of Medicine at Mount Sinai (STUDY-20-00341). Following written informed consent, 280 individuals were enrolled in the Mount Sinai COVID-19 cohort between April and June 2020 and had venous blood sampled for proteomics analysis at SomaLogic, Inc. (Boulder, CO). Included in this cohort were 198 patients hospitalized with COVID-19 and 82 controls, including 35 healthy controls and 47 patients hospitalized for reasons unrelated to COVID-19. Patients with acute COVID-19 were followed-up with 6 months or later [median: 414 days; interquartile range (IQR): 326 to 503] after COVID-19 hospital admission (fig. S1E). No further inclusion or exclusion criteria were applied on analysis of the 280 study participants with complete proteomics analysis and follow-up. Acute COVID-19 sampling was performed at a median time point of 1 day (IQR: 0 to 2) after hospital admission and before discharge. A subset of 21 patients underwent venous blood collection for further proteomics analysis after hospital discharge at a median time point of 89 days (IQR: 53 to 125) after hospital admission, i.e., 3-month follow-up (fig. S4F). Demographic characteristics of the cohort are given in table S3.

Definitions

Acute COVID-19 severity was graded according to recommendations of the World Health Organization (WHO) classification criteria into mild cases, including asymptomatic cases and patients with mild illness or pneumonia, and severe cases, consisting of patients with severe pneumonia, or mild, moderate, or severe acute respiratory distress syndrome (ARDS) (1, 18, 76). Symptomatic patients with uncomplicated SARS-CoV-2 infection, defined by an absence of abnormal vital signs and pathological lung examination findings, were classified as patients with mild illness, whereas patients with complicated SARS-CoV-2 infection, defined by the presence of one or more aforementioned criteria, were classified as patients with pneumonia. Patients with pneumonia requiring supplemental oxygen therapy, presenting with symptoms of severe respiratory distress, an increased respiratory rate (>30 breaths/min), and/or blood oxygen saturation levels below 93% on ambient air, were classified as patients with severe COVID-19. Severe COVID-19 patients were further classified on the basis of blood gas analysis ($\text{PaO}_2/\text{FiO}_2$ ratio) into severe pneumonia (>300 mmHg or unavailable), mild (<300 mmHg), moderate (<200 mmHg), and severe ARDS (<100 mmHg) (1, 18, 76). Acute COVID-19 severity was followed up until recovery or hospital release, thus, beyond the blood-sampling time point. Long Covid was defined as one or more persisting COVID-19-related symptoms, which could not be explained by an alternative diagnosis (2). In the present study, patients reporting isolated changes in

smell and/or taste were excluded from the Long Covid definition prior to analysis of the serum proteome, as pathomechanistic causes might be distinct in this patient subgroup (19). All reported symptoms are listed in table S1. Moreover, in accordance with the WHO clinical case definition of post COVID-19 condition (2), 6-month Long Covid and 12-month Long Covid were defined as persisting Long Covid symptoms at 6-month and 12-month follow-up, respectively. “Recovered Long Covid” included COVID-19 patients reporting one or more symptoms lasting for more than 4 weeks but no symptoms at 6-month follow-up (5, 77).

For the Mount Sinai cohort, 6-month Long Covid symptoms were defined in the same manner as for the Zurich cohort. These included fatigue, pulmonary symptoms, chest pain, gastrointestinal symptoms, cognitive symptoms, anxiety or depression, headache, and joint and muscle pain (table S3).

Serum processing and SomaScan proteomics

Following venous blood sampling, BD Vacutainer CAT serum tubes (Becton Dickinson, Franklin Lakes, NJ) were centrifuged at 1100g and 4°C for 10 min, followed by aliquotation and storage at -80°C. Thirty-nine serum samples of healthy controls and 113 paired serum samples of COVID-19 patients at acute COVID-19 and 6-month follow-up were used for proteomics analysis at SomaLogic using the SomaScan platform (version 4). Protein measurements were performed using 7335 modified single-stranded aptamers (SOMAmer reagents), including 7289 aptamers specific to 6596 unique human proteins and 46 internal controls, as previously described (20, 78). Protein epitope-SOMAmer reagent complexes were quantified by fluorescence using DNA-hybridization microarrays. All measurements passed manufacturer-defined quality control standards. Assay-intrinsic variation was corrected by median normalization using external references derived from 1025 healthy participants (79). Relative fluorescence units were log₁₀-transformed for analysis.

Mass spectrometry sample preparation, data acquisition, and processing

Samples were prepared as follows: 2.5 μl of the serum/plasma was transferred to a 0.5-ml 96-deepwell plate containing 27.5 μl denaturation/reduction buffer [8 M urea, 100 mM ammonium bicarbonate (ABC) and 46 mM dithiothreitol]. The plates were subsequently centrifuged for 20 s at pulse setting (Heraeus Multifuge X3R, Rotor TX-1000), mixed, and incubated at 30°C and 500 rpm for 60 min (Eppendorf Thermo-mixer C). Next, 2.5 μl of 100 mM chloroacetamide (CAA) was added to each sample, and the plate was incubated in the dark at 23°C and 500 rpm for 30 min (Eppendorf Thermo-mixer C). The samples were then diluted with 170 μl 100 mM ABC. Subsequently, 12.5 μl

trypsin solution (0.092 μg/μl) was added, and samples were incubated at 37°C and 500 rpm for 17 hours. Digestion was stopped by adding 10% formic acid (FA) to reach a final concentration of 1% FA. Peptides were desalted using an Oasis Prime HLB 96-well μElution Plate. Samples were loaded onto columns, washed twice with 400 μl 0.1% FA and once with 200 μl ddH₂O, and eluted with 50 μl 70% acetonitrile after a 1-min incubation at room temperature (RT). The liquid was evaporated with a SPD120 SpeedVac (Thermo Fisher Scientific), and samples were resuspended in 80 μl 0.1% FA, sonicated for 5 min in an ultrasonication water bath (Elmasonic P90), and centrifuged for 10 min at 3000 rpm and 4°C. Twenty microliters of the resulting samples was transferred to a 96-well plate, and 1 μl was injected.

Samples were acquired on an EASY-nLC 1200 coupled to a Thermo Orbitrap Eclipse Tribrid MS in data-independent acquisition (DIA) mode. Buffer A was 0.1% FA in water, and buffer B was 0.1% FA in 80% acetonitrile. A nanoLC column with integrated emitter from CoAnn Technologies with the following dimensions was used: 75 μm ID x 25 cm L x 365 μm OD, ReproSil-Pur120 C18 particles (1.9 μm). Further, an Acclaim PepMap 100 C18 pre-column (0.1 mm ID x 150 mm L with 5 μm particle size) was used. Flow rate was set to 200 nL/min, and the following gradient was applied: 45 min from 5% B to 31% B, 5 min from 31% B to 44% B, 1 min from 44% B to 95% B, 10 min hold at 95% B, 1 min from 95% B to 5% B, and 5 min equilibration at 5% B. For the MS1 scan, orbitrap resolution was set to 120,000, with quadrupole isolation turned on. A scan range of 380 to 980 m/z was applied, the RF lens was set to 30%, and standard automatic gain control (AGC) target with a custom maximum injection time of 50 ms was applied. For MS2 scan, orbitrap resolution was set to 15,000, with 50 fixed windows (12 m/z isolation window and 0.5 m/z overlap). Higher-energy collisional dissociation collision energy was fixed at 30%. MS/MS scan range was defined as 145 to 1450 m/z, and RF Lens was set to 30%. AGC Target was set to 1000% with custom maximum injection time of 22 ms.

Raw data was processed using DIA-NN software with default settings (80). Search was performed library-free with an *in silico* digestion and deep learning-based spectra and retention time prediction. The human fasta file was downloaded from UNIPROT (3AUP00005640Uniprot, downloaded on 7 September 2022). Downstream analysis was performed with R. For protein analysis, precursors were filtered for proteotypicity, precursor q-values were filtered with a threshold of 0.01, and protein group q-values were filtered with a threshold of 0.05. Only precursors quantified in >50% of samples were considered. Signal drifts were corrected by fitting a loess function for each precursor across the measurements (span = 0.7). Protein quanti-

ties were calculated using maxLFQ algorithm (maxLFQ function within DIA-NN R-package). For peptide level analysis of antithrombin III (gene name: SERPINC1), peptides with >10 observations measured per group (i.e., “no 6-month Long Covid” and “6-month Long Covid”) were summarized on the basis of their identical sequences, independently of differences in oxidation.

Protein and heme quantifications by ELISA, functional assays, and complete blood counts

Total C7 (AssayPro; Cat#EC7101-1), sC5b-9 (Quidel; Cat#A020), factor Ba (Quidel; Cat#A033), CH50 Equivalent (Quidel; Cat#A018), and vWF (AssayPro; Cat#CEV20301) were measured by applying commercially available ELISAs on patient sera analyzed with the SomaScan platform (39 healthy controls, and 113 COVID-19 patients at acute COVID-19 and 6-month follow-up), according to the manufacturers’ instructions. vWF measurements were calibrated against WHO controls. Factor Ba purified from human serum (CompTech; Cat#A154) was used as positive control. Six-month follow-up serum samples (*n* = 113) were used for measurements of PTX3 (AssayPro; Cat# EP2877-1) and heme (Sigma-Aldrich; Cat# MAK316). IL-6 serum concentrations were determined by ELISA (R&D Systems) on an Opsys Reader (Dynex). IL-6 measurements, hemoglobin, and complete blood counts were performed at an accredited laboratory of the University Hospital Zurich using serum or fresh whole blood.

C7-specific and SARS-CoV-2-specific IgG measurement

C7-specific autoantibodies were assessed using a previously described method (81). In brief, human C7 protein (Quidel; Cat#A405) diluted in phosphate-buffered saline (PBS) to 1 μg/ml was dispensed into high-binding 384-well SpectraPlates (Perkin Elmer) at 20 μl per well using Multidrop Combi nL (Thermo Fisher Scientific). Following coating overnight at 4°C, plates were washed three times with PBS Tween-20 0.1% (PBS-T) on a Bioteck El406 device using the 192-pin manifold. Forty microliters per well of blocking buffer (PBS-T with 5% milk powder) was dispensed, and plates were blocked for 1 hour at RT. Following removal of blocking agent, serial dilutions were done of serum samples (range: 0.02 to 2.74×10^{-5}) and of a polyclonal HRP-linked rabbit anti-human anti-C7 antibody as positive control (Novus Biologicals; Cat#NBP3-00202H; range: 4 to 8.4×10^{-7} μg/ml; fig. S2I), in sample buffer (PBS-T with 1% milk powder). Following incubation at RT for 2 hours, plates were washed five times. Twenty microliters per well of secondary antibody (HRP-conjugated goat anti-human IgG; Jackson), diluted 1:4000 in sample buffer, was dispensed into wells containing plasma samples, and 20 μl/well sample

buffer without secondary antibody into wells containing positive control using a Biotek Multiflo FX dispenser. After an incubation of 1 hour at RT and three wash cycles, 20 μ l/well TMB followed by 20 μ l/well 0.5 M H₂SO₄ were dispensed using an eight-pin manifold on a Certus Flex device (Fritz Gyger AG). The incubation time between the two reagents was 5 min.

SARS-CoV-2 spike-specific IgG was measured with the TRABI technology, as previously described (81), using wild-type/Wuhan SARS-CoV-2 spike extracellular domain, spike S1, spike S2 (AcroBiosystems; Cats#S1N-C52H2, S2N-C52H5), or receptor binding domain as antigens. The inflection points of sigmoidal binding curves [$-\log_{10}$ EC₅₀ or p(EC₅₀) values of respective sample dilutions] were determined using a custom-designed fitting algorithm, with plateau and baseline inferred from respective positive and negative controls in a plate-wise manner. Negative p(EC₅₀) values, reflecting nonreactive samples, were rescaled as zero. Samples included in C7-specific measurements were assayed and analyzed as duplicates, whereas SARS-CoV-2-specific measurements were conducted as unicates.

Antinuclear, anti-chemokine, and antiviral antibody quantifications

Antinuclear antibodies were measured by indirect immunofluorescence assays on HEp-2 cells using a computer-aided microscopy system (Euroimmun) at an accredited laboratory of the University Hospital Zurich, in a blinded manner, as previously reported (22). As positivity cutoff a dilution of 1:320 was applied. ANA patterns were classified on the basis of international consensus on ANA patterns anticell (AC) nomenclature (82).

Anti-chemokine antibodies were quantified by ELISA, as previously described (51). Anti-chemokine levels measured on 12-month follow-up samples of our cohort have been previously reported (51). For the present study, published data were reanalyzed in the context of 6-month Long Covid, by including only a subset of patients, for which we also had SomaScan and mass spectrometry measurements at 6-month follow-up available ($n = 88$, with 31 experiencing 6-month Long Covid).

For human virome-wide serological profiling by VirScan (22, 83), serum samples obtained at first study visit, including 57 acute COVID-19 patients (of which 22 developed 6-month Long Covid) and 18 healthy controls were measured, as previously reported (22). Briefly, duplicate serum samples were normalized for total IgG and incubated with a bacteriophage library displaying linear viral epitopes with lengths of 56 amino acids. IgG-phage complexes were isolated with magnetic beads and quantified by next-generation sequencing. Epitope hit counts were obtained using SAMtools (84) upon mapping of reads to the epitope library using Bowtie2 (85). Positivity for epitopes was

determined on the basis of a previously published binning strategy (86). Data on prokaryotes, eukaryotes, and nonhuman viruses, as well as human viruses with a maximal summed epitope hit count below three, were excluded.

For quantification of CMV- and EBV-specific IgM and IgG titers, ELISAs certified for diagnostic use were applied, according to the manufacturer's instruction, on 6-month follow-up serum samples of 113 COVID-19 patients (TestLine Clinical Diagnostics; Cats#CMM096, CMG096, VCM096, VCG096).

Anti-C7 aptamer ELISA, pull-down for SDS-PAGE, and Western blot analysis

For in vitro assembly of different TCC conformations, commercially available human recombinant C5bC6 (Sigma Aldrich; Cat#204906), C7 (Quidel; Cat#A405), C8 (Sigma Aldrich; Cat#204896), and C9 (Sigma Aldrich; Cat#204910) were mixed at an equimolar concentration (200 nM for pull-down) in SOMA1 buffer with Tween-20 buffer (120 mM NaCl, 5 mM KCl, 5 mM MgCl₂, 40 mM HEPES, pH 7.5, 0.05% Tween-20) and incubated overnight at 4°C.

For assessing C7 aptamer (seq.2888.49) specificity, streptavidin-coated plates (Thermo Fisher Scientific) were incubated overnight with the aptamer (20 nM diluted in SBT buffer). The next day, plates were blocked with 100 μ M biotin (10 min) and 3% bovine serum albumin (30 min) in SBT buffer. Upon addition of different combinations of TCCs C5bC6, C7, C8, and C9 at increasing concentrations (31.25 to 4000 ng/ml; 2 hours incubation), C7 was detected with a primary, polyclonal, full-length human C7-directed, rabbit antibody (Novus Biologicals; Cat#H00000730-D01P) and an HRP-linked secondary, goat, anti-rabbit IgG antibody (Cell Signaling Technologies; Cat#7074S). This experimental setup was repeated for measurement of monomeric C7 and of complexed C5b, C6, C7, C8, and C9 at different concentrations and in triplicates. To reduce unspecific aptamer–protein interactions, 1 μ M polyanionic competitor (SomaLogic) was added, reflecting similar conditions as the SomaScan platform.

For C7 aptamer-mediated pull-down of TCC components, Pierce Streptavidin magnetic beads (Thermo Scientific) were diluted in SBT buffer and mixed with 100 nM biotinylated C7 aptamer (SomaLogic, seq.2888.49) and incubated overnight at 4°C. The next day, beads were repeatedly washed with SBT buffer and mixed with complement protein solutions at a 1:1 ratio, together with 1 μ M polyanionic competitor (SomaLogic). After 2 hours of incubation, mixtures were washed with SBT buffer, and captured protein complexes were eluted from beads using 20 mM NaOH. Complement protein solutions were mixed with Laemmli sample buffer (BioRad) and incubated at 95°C for 5 min. Subsequently, samples were loaded on 4 to 20% polyacrylamide gels (BioRad). After separation, gels were

stained overnight using QuickBlue Protein Stain (Lubio science). Standard Western blotting protocol was applied. Rabbit anti-human C7 polyclonal antibodies (Novus Biologicals; Cat#H00000730-D01P) and HRP-linked goat anti-rabbit IgG antibodies (Cell Signaling Technologies; Cat#7074S) were used for detection. Acquisition was performed using Pierce ECL western substrate (Thermo Scientific) and imaged with a ChemiDoc Imaging System (BioRad).

Spectral flow cytometry and fluorescence-activated cell sorting (FACS)

Frozen PBMCs were thawed by slowly adding prewarmed RPMI medium (Gibco) containing 10% fetal bovine serum (FBS; Gibco). Cells were washed and stained, as previously published (11, 12). Briefly, after staining with ZombieUV Viability dye (1:400; BioLegend) and TruStain FcX (1:200) in PBS for 30 min at 4°C, surface antigens were stained with a mix of diluted fluorophore-conjugated antibodies (listed in data S6) in a 1:10 mixture of Brilliant Buffer (BD Bioscience) and FACS buffer (PBS containing 2% FBS and 2 mM EDTA) for 30 min at 4°C. Samples were acquired on a Cytek Aurora spectral flow cytometer. Gating strategy is shown in fig. S6A. Spectral flow cytometry data were analyzed using FlowJo (version 10.9.0). Dimensionality reduction and clustering were performed using the CATALYST (87) package in R (version 4.22). The dataset was reduced to 5000 randomly selected monocytes per patient to reduce required computational resources. Expression was scaled by hyperbolic arcsine transformation with a cofactor of 6000. UMAPs were calculated on CD14, CD16, CD11b, and CD36 levels using CATALYST. Monocytes were clustered using PhenoGraph clustering workflow of Rphenograph (88) package (version 0.99.1).

For sorting of monocytes using PBMC samples, staining was applied as described for the spectral flow cytometry analysis. In brief, cells were stained with fixable viability dye eFluor 780 (eBioscience) and TruStain FcX, followed by incubation with fluorescently labeled antibodies. For single-cell RNA sequencing, each sample was additionally barcoded with a hashtag antibody (data S6). For validation of monocyte-platelet aggregate staining by CD41, FACS-sorted (FACS Aria III 4L, BD Biosciences) monocytes were incubated with increasing counts of isolated platelets, with and without prestimulation of monocytes by LPS (10 ng/ml). Platelets were isolated from a healthy donor by centrifugation of EDTA blood, once at 1000g for 15 min and a second time at 13,000g for 5 min. Gating strategy is shown in fig. S6B.

Single-cell RNA sequencing

FACS-sorted PBMCs were immediately processed for further analysis by single-cell RNA sequencing. The resulting libraries were processed on an Illumina NovaSeq 6000 S1 flow

cell. Sequencing parameters were set according to 10X Genomics' recommendations, using paired-end reads with the following specifications: R1 = 26, i7 = 10, i5 = 10, and R2 = 90. An average depth of around 50,000 reads per cell was achieved. A custom reference genome was built to screen for herpesviral RNA transcripts by concatenating exogenous sequences in fasta format from NCBI to the human reference genome (build GRCh38.p13). Subsequently, the whole exogenous sequence was added to gene model (GENCODE Release 42) as an exon in GTF format, as recommended by 10X Genomics. The resulting hybrid fasta and GTF files were used as inputs to generate a 10X-compatible reference genome using *CellRanger* (v7.1.0) *mkfastq* (89). The *CellRanger* pipeline was used for demultiplexing, read alignment to the custom reference, barcode processing, and unique molecular identifier (UMI) counting. Custom references are listed in data S7.

Subsequent data analysis was performed in R. Single cells were mapped to a PBMC reference dataset (version 1.0.0) (90) using *Seurat* (version 4.3.0) (91), as described in the multimodal reference mapping vignette. Differential gene expression analysis of monocytes was performed using the *Seurat* package.

Gene set enrichment analysis, association analysis, and random forest prediction model

Univariate association analysis of protein-aptamer concentrations to binary 6-month Long Covid endpoints was performed using logistic regression, adjusting for patient age, sex, and hospitalization status (6-month Long Covid ~ aptamer xyz + patient age [numeric] + sex [female/male] + hospitalization during acute COVID-19 [yes/no] + intercept constant), implemented as the python Statsmodels API Logit class. Analyses were performed with respect to either acute COVID-19 or 6-month follow-up measurements. The obtained *P* values for the individual aptamers were used for further analysis, such as differential expression and ranking of protein concentrations for enrichment analysis. For gene set enrichment analysis, duplicate measurements of proteins, resulting from multiple aptamers targeting the same protein, were selected on the basis of the lowest *P* value of competing aptamers, resulting in 6408 aptamers with unique Entrez Gene ID's. Subsequently, these 6408 human proteins were ranked by multiplying univariate association $-\log_{10}$ -transformed *P* values with the sign of recorded fold changes. Gene set enrichment analysis was performed using the *fgsea* R package with Reactome pathways (26, 92).

Biological protein clusters were selected on the basis of protein measurement availability and maximizing uniqueness and representativeness for the respective pathways and protein groups according to the literature (table S2). Biological protein cluster associations with

6-month Long Covid were assessed by association analysis through logistic regression, with all protein levels of a specific cluster or pathway being used as model inputs, in addition to patient age, sex, and hospitalization status. Relevant *P* values in these analyses represented the log likelihood ratios (LLR) of the model as a whole. For associations, we determined a Bonferroni-corrected significance threshold of $P < 6.80 \times 10^{-6}$, corresponding to a *P* value of 0.05 divided by 7353, including all 7335 aptamer measurements and 18 biological protein clusters.

Finally, binary predictions of 6- and 12-month Long Covid were performed using a random forest classifier implemented using the *sklearn RandomForestClassifier* (93). Input data were obtained at acute COVID-19 or 6-month follow-up and comprised all SomaScan proteomic measurements, four protein ratios based on biological reasoning and published literature (C5/C7 complexes, C5bC6/C7 complexes, vWF/ADAMTS13, and angiopoietin-2/angiopoietin-1), and 14 general clinical variables assessed at acute COVID-19 or 6-month follow-up. We purposely excluded clinical variables on COVID-19 history, as this information may not be available for patients assessed for Long Covid diagnosis in a clinical setting. Of 7289 aptamer measurements, 61 uncorrelated measurements (with absolute Spearman correlation coefficient values below 0.3) were selected together with two uncorrelated protein ratios, and 14 clinical variables for prediction of 6-month Long Covid versus no 6-month Long Covid and healthy controls ($n = 40$, 73, and 39, respectively) with acute COVID-19 or 6-month follow-up data. We performed stratified (for patient age group [<60 years/ >60 years] and acute COVID severity [mild/severe]) fivefold nested cross-validation using 20% of the samples for testing, and inner fivefold cross-validation for hyperparameter tuning by *GridSearch* optimizing tree depth, number of leaves, sample splits, and maximum number of features. All models were trained with balanced class weights and results were reported as mean values and standard deviations of independent test sets in terms of AUROC and relative average precision scores, reflecting the area under the precision recall curve normalized by positive class prevalence. The latter score indicates the improvement beyond a random classifier for values exceeding unity. To infer features that drove predictions, we performed post-hoc interpretability analysis using SHapley Additive exPlanations as part of the python *shap* package (94). We reported an agglomerated interpretation overview in terms of summed ranks of individual fivefold cross-validation interpretations. The top features obtained in this analysis and identified by visual inspection of an elbow plot were selected for reevaluation in the prediction task, as outlined above. Importantly, the

identified top four features were selected on training data allowing further predictions followed by evaluation on test data.

Visualization and statistics

Descriptive statistics for the study participants are reported in numbers and percentages of total for categorical as well as median and IQR for continuous variables. Comparison of paired variables was performed using Wilcoxon's signed-rank test and comparison of nonpaired variables was performed using nonparametric two-sided Wilcoxon's rank-sum test. Split violin plots overlayed with boxplots visualize median and quartiles. Correlations were calculated using Spearman's correlation in R. Differential expression in volcano plots was calculated using *t* tests, Wilcoxon's rank-sum test, or logistic regression, as specified. *P* values were $-\log_{10}$ -transformed and fold changes \log_2 -transformed. Multiple testing was corrected by Benjamini-Hochberg (95) or Bonferroni correction, as specified. Statistical analysis was performed with R studio (version 2023.03.1) and R (version 4.1.2) using the packages *SomaDataIO*, *fgsea*, *pheatmap*, *corrplot* (96), *lmerTest* (97), *VennDiagram*, and *tidyverse* (98) as well as python (version 3.7.4) using the packages *Numpy*, *Openpyxl*, *Scipy*, *Pandas*, *Scikit-learn*, *Statsmodels* (99), and *Shap*. Acute COVID-19 and 6-month follow-up clinical and SomaScan data contained no missing values. ELISA validation experiments contained a total of three to seven missing values. The number of observations per analysis are listed in data S9. The present study is reported according to the STROBE (Statement for reporting cohort studies) guidelines (100).

REFERENCES AND NOTES

1. World Health Organization, COVID-19 Clinical management: interim guidance, 27 May 2020 (World Health Organization, 2020); <https://apps.who.int/iris/handle/10665/332196>.
2. World Health Organization, A clinical case definition of post COVID-19 condition by a Delphi consensus, 6 October 2021 (World Health Organization, 2021); https://www.who.int/publications/item/WHO-2019-nCoV-Post_COVID-19_condition-Clinical_case_definition-2021.
3. Global Burden of Disease Long COVID Collaborators. Estimated global proportions of individuals with persistent fatigue, cognitive, and respiratory symptom clusters following symptomatic COVID-19 in 2020 and 2021. *JAMA* **328**, 1604–1615 (2022). doi: [10.1001/jama.2022.18931](https://doi.org/10.1001/jama.2022.18931); pmid: [36215063](https://pubmed.ncbi.nlm.nih.gov/36215063/)
4. D. Menges et al., Burden of post-COVID-19 syndrome and implications for healthcare service planning: A population-based cohort study. *PLOS ONE* **16**, e0254523 (2021). doi: [10.1371/journal.pone.0254523](https://doi.org/10.1371/journal.pone.0254523); pmid: [34252157](https://pubmed.ncbi.nlm.nih.gov/34252157/)
5. W. Shah, T. Hillman, E. D. Playford, L. Hishmeh, Managing the long term effects of covid-19: Summary of NICE, SIGN, and RCGP rapid guideline. *BMJ* **372**, n136 (2021). doi: [10.1136/bmj.n136](https://doi.org/10.1136/bmj.n136); pmid: [33483331](https://pubmed.ncbi.nlm.nih.gov/33483331/)
6. C. Kedor et al., A prospective observational study of post-COVID-19 chronic fatigue syndrome following the first pandemic wave in Germany and biomarkers associated with symptom severity. *Nat. Commun.* **13**, 5104 (2022). doi: [10.1038/s41467-022-32507-6](https://doi.org/10.1038/s41467-022-32507-6); pmid: [36042189](https://pubmed.ncbi.nlm.nih.gov/36042189/)
7. H. E. Davis, L. McCorkell, J. M. Vogel, E. J. Topol, Long COVID: Major findings, mechanisms and recommendations. *Nat. Rev. Microbiol.* **21**, 133–146 (2023). doi: [10.1038/s41579-022-00846-2](https://doi.org/10.1038/s41579-022-00846-2); pmid: [36639608](https://pubmed.ncbi.nlm.nih.gov/36639608/)

8. S. Chevrier et al., A distinct innate immune signature marks progression from mild to severe COVID-19. *Cell Rep. Med.* **2**, 100166 (2020). doi: [10.11016/j.xcrm.2020.100166](https://doi.org/10.11016/j.xcrm.2020.100166); pmid: [33521697](https://pubmed.ncbi.nlm.nih.gov/33521697/)
9. A. K. Azkur et al., Immune response to SARS-CoV-2 and mechanisms of immunopathological changes in COVID-19. *Allergy* **75**, 1564–1581 (2020). doi: [10.1111/all.13464](https://doi.org/10.1111/all.13464); pmid: [32396996](https://pubmed.ncbi.nlm.nih.gov/32396996/)
10. C. Cervia et al., Systemic and mucosal antibody responses specific to SARS-CoV-2 during mild versus severe COVID-19. *J. Allergy Clin. Immunol.* **147**, 545–557.e9 (2021). doi: [10.11016/j.jaci.2020.10.040](https://doi.org/10.11016/j.jaci.2020.10.040); pmid: [33221383](https://pubmed.ncbi.nlm.nih.gov/33221383/)
11. S. Adamo et al., Signature of long-lived memory CD8⁺ T cells in acute SARS-CoV-2 infection. *Nature* **602**, 148–155 (2022). doi: [10.1038/s41586-021-04280-x](https://doi.org/10.1038/s41586-021-04280-x); pmid: [34875673](https://pubmed.ncbi.nlm.nih.gov/34875673/)
12. Y. Zurbuchen et al., Human memory B cells show plasticity and adopt multiple fates upon recall response to SARS-CoV-2. *Nat. Immunol.* **24**, 955–965 (2023). doi: [10.1038/s41590-023-01497-y](https://doi.org/10.1038/s41590-023-01497-y); pmid: [37106039](https://pubmed.ncbi.nlm.nih.gov/37106039/)
13. C. Cervia et al., Immunoglobulin signature predicts risk of post-acute COVID-19 syndrome. *Nat. Commun.* **13**, 446 (2022). doi: [10.1038/s41467-021-27797-1](https://doi.org/10.1038/s41467-021-27797-1); pmid: [35078982](https://pubmed.ncbi.nlm.nih.gov/35078982/)
14. S. Guenther et al., Frequent IgG subclass and mannose binding lectin deficiency in patients with chronic fatigue syndrome. *Hum. Immunol.* **76**, 729–735 (2015). doi: [10.11016/j.humimm.2015.09.028](https://doi.org/10.11016/j.humimm.2015.09.028); pmid: [26429318](https://pubmed.ncbi.nlm.nih.gov/26429318/)
15. R. C. Thompson et al., Molecular states during acute COVID-19 reveal distinct etiologies of long-term sequelae. *Nat. Med.* **29**, 236–246 (2023). doi: [10.1038/s41591-022-02107-4](https://doi.org/10.1038/s41591-022-02107-4); pmid: [36482101](https://pubmed.ncbi.nlm.nih.gov/36482101/)
16. L. Perico et al., Immunity, endothelial injury and complement-induced coagulopathy in COVID-19. *Nat. Rev. Nephrol.* **17**, 46–64 (2021). doi: [10.1038/s41581-020-00357-4](https://doi.org/10.1038/s41581-020-00357-4); pmid: [33077917](https://pubmed.ncbi.nlm.nih.gov/33077917/)
17. M. Merad, C. A. Blish, F. Sallusto, A. Iwasaki, The immunology and immunopathology of COVID-19. *Science* **375**, 1122–1127 (2022). doi: [10.1126/science.abm8108](https://doi.org/10.1126/science.abm8108); pmid: [35271343](https://pubmed.ncbi.nlm.nih.gov/35271343/)
18. World Health Organization, COVID-19 Clinical management: living guidance, 25 January 2021 (World Health Organization, 2021); <https://iris.who.int/bitstream/handle/10665/338882/WHO-2019-nCoV-clinical-2021-eng.pdf>
19. J. F. Shelton, A. J. Shastri, K. Fletez-Brant, S. Aslzbekyan, A. Auton; 23andMe COVID-19 Team, The UGT2A1/UGT2A2 locus is associated with COVID-19-related loss of smell or taste. *Nat. Genet.* **54**, 121–124 (2022). doi: [10.1038/s41588-021-00986-w](https://doi.org/10.1038/s41588-021-00986-w); pmid: [35039640](https://pubmed.ncbi.nlm.nih.gov/35039640/)
20. L. Gold et al., Aptamer-based multiplexed proteomic technology for biomarker discovery. *PLOS ONE* **5**, e15004 (2010). doi: [10.1371/journal.pone.0015004](https://doi.org/10.1371/journal.pone.0015004); pmid: [21165148](https://pubmed.ncbi.nlm.nih.gov/21165148/)
21. S. E. Chang et al., New-onset IgG autoantibodies in hospitalized patients with COVID-19. *Nat. Commun.* **12**, 5417 (2021). doi: [10.1038/s41467-021-25509-3](https://doi.org/10.1038/s41467-021-25509-3); pmid: [34521836](https://pubmed.ncbi.nlm.nih.gov/34521836/)
22. P. Taeschler et al., Autoantibodies in COVID-19 correlate with antiviral humoral responses and distinct immune signatures. *Allergy* **77**, 2415–2430 (2022). doi: [10.1111/all.15302](https://doi.org/10.1111/all.15302); pmid: [35364615](https://pubmed.ncbi.nlm.nih.gov/35364615/)
23. PHOSP-COVID Collaborative Group, Clinical characteristics with inflammation profiling of long COVID and association with 1-year recovery following hospitalisation in the UK: A prospective observational study. *Lancet Respir. Med.* **10**, 761–775 (2022). doi: [10.1016/S2213-2600\(22\)00127-8](https://doi.org/10.1016/S2213-2600(22)00127-8); pmid: [35472304](https://pubmed.ncbi.nlm.nih.gov/35472304/)
24. P. Taeschler et al., T-cell recovery and evidence of persistent immune activation 12 months after severe COVID-19. *Allergy* **77**, 2468–2481 (2022). doi: [10.1111/all.15372](https://doi.org/10.1111/all.15372); pmid: [35567391](https://pubmed.ncbi.nlm.nih.gov/35567391/)
25. B. Blomberg et al., Long COVID in a prospective cohort of home-isolated patients. *Nat. Med.* **27**, 1607–1613 (2021). doi: [10.1038/s41591-021-01433-3](https://doi.org/10.1038/s41591-021-01433-3); pmid: [34163090](https://pubmed.ncbi.nlm.nih.gov/34163090/)
26. M. Gillespie et al., The reactome pathway knowledgebase 2022. *Nucleic Acids Res.* **50**, D687–D692 (2022). doi: [10.1093/nar/gkab1028](https://doi.org/10.1093/nar/gkab1028); pmid: [34788843](https://pubmed.ncbi.nlm.nih.gov/34788843/)
27. J. V. Sarma, P. A. Ward, The complement system. *Cell Tissue Res.* **343**, 227–235 (2011). doi: [10.1007/s00441-010-1034-0](https://doi.org/10.1007/s00441-010-1034-0); pmid: [20838815](https://pubmed.ncbi.nlm.nih.gov/20838815/)
28. A. Mantovani, C. Garlanda, Humoral innate immunity and acute-phase proteins. *N. Engl. J. Med.* **388**, 439–452 (2023). doi: [10.1056/NEJMra2206346](https://doi.org/10.1056/NEJMra2206346); pmid: [36724330](https://pubmed.ncbi.nlm.nih.gov/36724330/)
29. R. Würzner et al., Functionally active complement proteins C6 and C7 detected in C6- and C7-deficient individuals. *Clin. Exp. Immunol.* **83**, 430–437 (1991). doi: [10.1111/j.1365-2249.1991.tb05656.x](https://doi.org/10.1111/j.1365-2249.1991.tb05656.x); pmid: [2004484](https://pubmed.ncbi.nlm.nih.gov/2004484/)
30. R. Würzner, Modulation of complement membrane attack by local C7 synthesis. *Clin. Exp. Immunol.* **121**, 8–10 (2000). doi: [10.1046/j.1365-2249.2000.01263.x](https://doi.org/10.1046/j.1365-2249.2000.01263.x); pmid: [10886232](https://pubmed.ncbi.nlm.nih.gov/10886232/)
31. F. Bossi et al., C7 is expressed on endothelial cells as a trap for the assembling terminal complement complex and may exert anti-inflammatory function. *Blood* **113**, 3640–3648 (2009). doi: [10.1182/blood-2008-03-146472](https://doi.org/10.1182/blood-2008-03-146472); pmid: [19179470](https://pubmed.ncbi.nlm.nih.gov/19179470/)
32. L. Ma et al., Increased complement activation is a distinctive feature of severe SARS-CoV-2 infection. *Sci. Immunol.* **6**, eabb2259 (2021). doi: [10.1126/sciimmuno.abb2259](https://doi.org/10.1126/sciimmuno.abb2259); pmid: [34446527](https://pubmed.ncbi.nlm.nih.gov/34446527/)
33. M. Huber-Lang et al., Generation of C5a in the absence of C3: A new complement activation pathway. *Nat. Med.* **12**, 682–687 (2006). doi: [10.1038/nm1419](https://doi.org/10.1038/nm1419); pmid: [16715088](https://pubmed.ncbi.nlm.nih.gov/16715088/)
34. M. J. Krisinger et al., Thrombin generates previously unidentified C5 products that support the terminal complement activation pathway. *Blood* **120**, 1717–1725 (2012). doi: [10.1182/blood-2012-02-412080](https://doi.org/10.1182/blood-2012-02-412080); pmid: [22802338](https://pubmed.ncbi.nlm.nih.gov/22802338/)
35. D. A. Lane, R. Caso, Antithrombin: Structure, genomic organization, function and inherited deficiency. *Baillieres Clin. Haematol.* **2**, 961–998 (1989). doi: [10.1016/S0953-5369\(89\)80054-X](https://doi.org/10.1016/S0953-5369(89)80054-X); pmid: [2688761](https://pubmed.ncbi.nlm.nih.gov/2688761/)
36. A. R. Rezaie, H. Giri, Anticoagulant and signaling functions of antithrombin. *J. Thromb. Haemost.* **18**, 3142–3153 (2020). doi: [10.1111/jth.15052](https://doi.org/10.1111/jth.15052); pmid: [32809336](https://pubmed.ncbi.nlm.nih.gov/32809336/)
37. S. Pillarisetti, Lipoprotein modulation of subendothelial heparan sulfate proteoglycans (perlecan) and atherogenicity. *Trends Cardiovasc. Med.* **10**, 60–65 (2000). doi: [10.1016/S1050-1738\(00\)00048-7](https://doi.org/10.1016/S1050-1738(00)00048-7); pmid: [1150731](https://pubmed.ncbi.nlm.nih.gov/1150731/)
38. D. Ricklin, E. S. Reis, J. D. Lambris, Complement in disease: A defence system turning offensive. *Nat. Rev. Nephrol.* **12**, 383–401 (2016). doi: [10.1038/nrneph.2016.70](https://doi.org/10.1038/nrneph.2016.70); pmid: [27211870](https://pubmed.ncbi.nlm.nih.gov/27211870/)
39. S. P. Jackson, R. Darboussat, S. M. Schoenwaelder, Thromboinflammation: Challenges of therapeutically targeting coagulation and other host defense mechanisms. *Blood* **133**, 906–918 (2019). doi: [10.1182/blood-2018-11-882993](https://doi.org/10.1182/blood-2018-11-882993); pmid: [30642917](https://pubmed.ncbi.nlm.nih.gov/30642917/)
40. L. Camous et al., Complement alternative pathway acts as a positive feedback amplification of neutrophil activation. *Blood* **117**, 1340–1349 (2011). doi: [10.1182/blood-2010-05-283564](https://doi.org/10.1182/blood-2010-05-283564); pmid: [21063021](https://pubmed.ncbi.nlm.nih.gov/21063021/)
41. J. Zhang, Biomarkers of endothelial activation and dysfunction in cardiovascular diseases. *Rev. Cardiovasc. Med.* **23**, 73 (2022). doi: [10.31083/jrcm2302073](https://doi.org/10.31083/jrcm2302073); pmid: [35229564](https://pubmed.ncbi.nlm.nih.gov/35229564/)
42. J. R. Delanghe, M. R. Langlois, Hemopexin: A review of biological aspects and the role in laboratory medicine. *Clin. Chim. Acta* **312**, 12–23 (2001). doi: [10.1016/S0009-8981\(01\)00586-1](https://doi.org/10.1016/S0009-8981(01)00586-1); pmid: [11580905](https://pubmed.ncbi.nlm.nih.gov/11580905/)
43. S. Wang et al., S100A8/A9 in inflammation. *Front. Immunol.* **9**, 1298 (2018). doi: [10.3389/fimmu.2018.01298](https://doi.org/10.3389/fimmu.2018.01298); pmid: [29942307](https://pubmed.ncbi.nlm.nih.gov/29942307/)
44. G. Baidildinova et al., Soluble platelet release factors as biomarkers for cardiovascular disease. *Front. Cardiovasc. Med.* **8**, 684920 (2021). doi: [10.3389/fcvm.2021.684920](https://doi.org/10.3389/fcvm.2021.684920); pmid: [34235190](https://pubmed.ncbi.nlm.nih.gov/34235190/)
45. S. Kamath, A. D. Blann, G. Y. Lip, Platelet activation: Assessment and quantification. *Eur. Heart J.* **22**, 1561–1571 (2001). doi: [10.1053/euhj.2000.2515](https://doi.org/10.1053/euhj.2000.2515); pmid: [11492985](https://pubmed.ncbi.nlm.nih.gov/11492985/)
46. D. M. Smadja et al., Thrombospondin-1 is a plasmatic marker of peripheral arterial disease that modulates endothelial progenitor cell angiogenic properties. *Arterioscler. Thromb. Vasc. Biol.* **31**, 551–559 (2011). doi: [10.1161/ATVBAHA.110.220624](https://doi.org/10.1161/ATVBAHA.110.220624); pmid: [21484243](https://pubmed.ncbi.nlm.nih.gov/21484243/)
47. J. Chen, D. W. Chung, Inflammation, von Willebrand factor, and ADAMTS13. *Blood* **132**, 141–147 (2018). doi: [10.1182/blood-2018-02-769000](https://doi.org/10.1182/blood-2018-02-769000); pmid: [29866815](https://pubmed.ncbi.nlm.nih.gov/29866815/)
48. A. Marco, P. Marco, Von Willebrand factor and ADAMTS13 activity as clinical severity markers in patients with COVID-19. *J. Thromb. Thrombolysis* **52**, 497–503 (2021). doi: [10.1007/s11239-021-02457-9](https://doi.org/10.1007/s11239-021-02457-9); pmid: [33866481](https://pubmed.ncbi.nlm.nih.gov/33866481/)
49. M. Lu, Q. Lu, Y. Zhang, G. Tian, ApoB/apoA1 is an effective predictor of coronary heart disease risk in overweight and obesity. *J. Biomed. Res.* **25**, 266–273 (2011). doi: [10.1016/S1674-8301\(11\)60036-5](https://doi.org/10.1016/S1674-8301(11)60036-5); pmid: [23554700](https://pubmed.ncbi.nlm.nih.gov/23554700/)
50. A. K. Maher et al., Transcriptional reprogramming from innate immune functions to a pro-thrombotic signature by monocytes in COVID-19. *Nat. Commun.* **13**, 7947 (2022). doi: [10.1038/s41467-022-35638-y](https://doi.org/10.1038/s41467-022-35638-y); pmid: [36572683](https://pubmed.ncbi.nlm.nih.gov/36572683/)
51. J. Muri et al., Autoantibodies against chemokines post-SARS-CoV-2 infection correlate with disease course. *Nat. Immunol.* **24**, 604–611 (2023). doi: [10.1038/s41590-023-01445-w](https://doi.org/10.1038/s41590-023-01445-w); pmid: [36879067](https://pubmed.ncbi.nlm.nih.gov/36879067/)
52. Y. Su et al., Multiple early factors anticipate post-acute COVID-19 sequelae. *Cell* **185**, 881–895.e20 (2022). doi: [10.1016/j.cell.2022.01.014](https://doi.org/10.1016/j.cell.2022.01.014); pmid: [35216672](https://pubmed.ncbi.nlm.nih.gov/35216672/)
53. M. L. Gulley, Molecular diagnosis of Epstein-Barr virus-related diseases. *J. Mol. Diagn.* **3**, 1–10 (2001). doi: [10.1016/S1525-1578\(10\)60642-3](https://doi.org/10.1016/S1525-1578(10)60642-3); pmid: [11227065](https://pubmed.ncbi.nlm.nih.gov/11227065/)
54. E. Callaway, Beyond Omicron: What's next for COVID's viral evolution. *Nature* **600**, 204–207 (2021). doi: [10.1038/d41586-021-03619-8](https://doi.org/10.1038/d41586-021-03619-8); pmid: [34876665](https://pubmed.ncbi.nlm.nih.gov/34876665/)
55. Office for National Statistics, Prevalence of ongoing symptoms following coronavirus (COVID-19) infection in the UK: 1 June 2022, Statistical Bulletin (2022); <https://www.ons.gov.uk/peoplepopulationandcommunity/healthandsocialcare/conditionsanddiseases/bulletins/prevalenceofongoingsymptomsfollowingcoronaviruscovid19infectionintheuk/1june2022>.
56. H. Kröning et al., ICAM G241A polymorphism and soluble ICAM-1 serum levels: Evidence for an active immune process in schizophrenia. *Neuroimmunomodulation* **12**, 54–59 (2005). doi: [10.1159/000082364](https://doi.org/10.1159/000082364); pmid: [15756053](https://pubmed.ncbi.nlm.nih.gov/15756053/)
57. S.-H. Yun, E.-H. Sim, R.-Y. Goh, J.-I. Park, J.-Y. Han, Platelet activation: the mechanisms and potential biomarkers. *BioMed Res. Int.* **2016**, 9060143 (2016). doi: [10.1155/2016/9060143](https://doi.org/10.1155/2016/9060143); pmid: [27403440](https://pubmed.ncbi.nlm.nih.gov/27403440/)
58. L. M. Carlin et al., Nr4a1-dependent Ly6C^{low} monocytes monitor endothelial cells and orchestrate their disposal. *Cell* **153**, 362–375 (2013). doi: [10.11016/j.cell.2013.03.010](https://doi.org/10.11016/j.cell.2013.03.010); pmid: [23582326](https://pubmed.ncbi.nlm.nih.gov/23582326/)
59. J. S. Lee, E.-C. Shin, The type I interferon response in COVID-19: Implications for treatment. *Nat. Rev. Immunol.* **20**, 585–586 (2020). doi: [10.1038/s41577-020-00429-3](https://doi.org/10.1038/s41577-020-00429-3); pmid: [32788708](https://pubmed.ncbi.nlm.nih.gov/32788708/)
60. M. C. Dalakas, H. Alexopoulos, P. J. Spaeth, Complement in neurological disorders and emerging complement-targeted therapeutics. *Nat. Rev. Neurol.* **16**, 601–617 (2020). doi: [10.1038/s41586-020-0400-0](https://doi.org/10.1038/s41586-020-0400-0); pmid: [33005040](https://pubmed.ncbi.nlm.nih.gov/33005040/)
61. A. Smith, R. J. McCullough, Hemopexin and haptoglobin: Allies against heme toxicity from hemoglobin not contenders. *Front. Physiol.* **6**, 187 (2015). doi: [10.3389/fphys.2015.00187](https://doi.org/10.3389/fphys.2015.00187); pmid: [26175690](https://pubmed.ncbi.nlm.nih.gov/26175690/)
62. B.-N. Wan, S.-G. Zhou, M. Wang, X. Zhang, G. Ji, Progress on haptoglobin and metabolic diseases. *World J. Diabetes* **12**, 206–214 (2021). doi: [10.4239/wjd.v12.i3.206](https://doi.org/10.4239/wjd.v12.i3.206); pmid: [33758643](https://pubmed.ncbi.nlm.nih.gov/33758643/)
63. M. Stravalaci et al., Recognition and inhibition of SARS-CoV-2 by humoral innate immunity pattern recognition molecules. *Nat. Immunol.* **23**, 275–286 (2022). doi: [10.1038/s41590-021-0114-w](https://doi.org/10.1038/s41590-021-0114-w); pmid: [35102342](https://pubmed.ncbi.nlm.nih.gov/35102342/)
64. A. Rajamanickam et al., Levels of complement components in children with acute COVID-19 or multisystem inflammatory syndrome. *JAMA Netw. Open* **6**, e231713 (2023). doi: [10.1001/jamanetworkopen.2023.1713](https://doi.org/10.1001/jamanetworkopen.2023.1713); pmid: [36961465](https://pubmed.ncbi.nlm.nih.gov/36961465/)
65. E. Brunetta et al., Macrophage expression and prognostic significance of the long pentraxin PTX3 in COVID-19. *Nat. Immunol.* **22**, 19–24 (2021). doi: [10.1038/s41038-019-0245-9](https://doi.org/10.1038/s41038-019-0245-9); pmid: [34208929](https://pubmed.ncbi.nlm.nih.gov/34208929/)
66. C. Phetsouphanh et al., Immunological dysfunction persists for 8 months following initial mild-to-moderate SARS-CoV-2 infection. *Nat. Immunol.* **23**, 210–216 (2022). doi: [10.1038/s41590-021-01113-x](https://doi.org/10.1038/s41590-021-01113-x); pmid: [35027728](https://pubmed.ncbi.nlm.nih.gov/35027728/)
67. B. Afzali, M. Noris, B. N. Lambrecht, C. Kemper, The state of complement in COVID-19. *Nat. Rev. Immunol.* **22**, 77–84 (2022). doi: [10.1038/s41577-021-00665-1](https://doi.org/10.1038/s41577-021-00665-1); pmid: [34912108](https://pubmed.ncbi.nlm.nih.gov/34912108/)
68. B. Yan et al., SARS-CoV-2 drives JAK1/2-dependent local complement hyperactivation. *Sci. Immunol.* **6**, eabb0833 (2021). doi: [10.1126/sciimmunol.abg0833](https://doi.org/10.1126/sciimmunol.abg0833); pmid: [33827897](https://pubmed.ncbi.nlm.nih.gov/33827897/)
69. J. Cousin-Frankel, Clues to Long Covid. *Science* **376**, 1261–1265 (2022). doi: [10.1126/science.add4297](https://doi.org/10.1126/science.add4297); pmid: [35709281](https://pubmed.ncbi.nlm.nih.gov/35709281/)
70. C. Wang et al., Long COVID: The nature of thrombotic sequelae determines the necessity of early anticoagulation. *Front. Cell. Infect. Microbiol.* **12**, 861703 (2022). doi: [10.3389/fcimb.2022.861703](https://doi.org/10.3389/fcimb.2022.861703); pmid: [35449732](https://pubmed.ncbi.nlm.nih.gov/35449732/)
71. P. Ambrosino et al., Persistent endothelial dysfunction in post-acute COVID-19 syndrome: a case-control study. *Biomaterials* **9**, 957 (2021). doi: [10.3390/biomaterials9080957](https://doi.org/10.3390/biomaterials9080957); pmid: [34440161](https://pubmed.ncbi.nlm.nih.gov/34440161/)
72. M. H. Lee et al., Neurovascular injury with complement activation and inflammation in COVID-19. *Brain* **145**, 2555–2568 (2022). doi: [10.1093/brain/awac151](https://doi.org/10.1093/brain/awac151); pmid: [35788639](https://pubmed.ncbi.nlm.nih.gov/35788639/)
73. A. Constantinescu-Bercu et al., Analysis of thrombogenicity under flow reveals new insights into the prothrombotic state

- of patients with post-COVID syndrome. *J. Thromb. Haemost.* **21**, 94–100 (2023). doi: [10.1016/j.jtha.2022.10.013](https://doi.org/10.1016/j.jtha.2022.10.013); pmid: [36695401](#)
74. E. Pretorius *et al.*, Persistent clotting protein pathology in Long COVID/Post-Acute Sequelae of COVID-19 (PASC) is accompanied by increased levels of antiplasmin. *Cardiovasc. Diabetol.* **20**, 172 (2021). doi: [10.1186/s12933-021-01359-7](https://doi.org/10.1186/s12933-021-01359-7); pmid: [34425843](#)
75. Y. Xie, E. Xu, B. Bowe, Z. Al-Aly, Long-term cardiovascular outcomes of COVID-19. *Nat. Med.* **28**, 583–590 (2022). doi: [10.1038/s41591-022-01689-3](https://doi.org/10.1038/s41591-022-01689-3); pmid: [35132265](#)
76. ARDS Definition Task Force, Acute respiratory distress syndrome: The Berlin Definition. *JAMA* **307**, 2526–2533 (2012). pmid: [22797452](#)
77. A. Nalbandian *et al.*, Post-acute COVID-19 syndrome. *Nat. Med.* **27**, 601–615 (2021). doi: [10.1038/s41591-021-01283-z](https://doi.org/10.1038/s41591-021-01283-z); pmid: [33753937](#)
78. B. B. Sun *et al.*, Genomic atlas of the human plasma proteome. *Nature* **558**, 73–79 (2018). doi: [10.1038/s41586-018-0175-2](https://doi.org/10.1038/s41586-018-0175-2); pmid: [29875488](#)
79. S. A. Williams *et al.*, Plasma protein patterns as comprehensive indicators of health. *Nat. Med.* **25**, 1851–1857 (2019). doi: [10.1038/s41591-019-0665-2](https://doi.org/10.1038/s41591-019-0665-2); pmid: [31792462](#)
80. V. Demichev, C. B. Messner, S. I. Vernardis, K. S. Lilley, M. Ralser, DIA-NN: Neural networks and interference correction enable deep proteome coverage in high throughput. *Nat. Methods* **17**, 41–44 (2020). doi: [10.1038/s41592-019-0638-x](https://doi.org/10.1038/s41592-019-0638-x); pmid: [31768060](#)
81. M. Emmenegger *et al.*, Continuous population-level monitoring of SARS-CoV-2 seroprevalence in a large European metropolitan region. *iScience* **26**, 105928 (2023). doi: [10.1016/j.isci.2023.105928](https://doi.org/10.1016/j.isci.2023.105928); pmid: [36619367](#)
82. E. K. L. Chan *et al.*, Report of the First International Consensus on Standardized Nomenclature of Antinuclear Antibody HEp-2 Cell Patterns 2014–2015. *Front. Immunol.* **6**, 412 (2015). doi: [10.3389/fimmu.2015.00412](https://doi.org/10.3389/fimmu.2015.00412); pmid: [26347739](#)
83. C. Pou *et al.*, The repertoire of maternal anti-viral antibodies in human newborns. *Nat. Med.* **25**, 591–596 (2019). doi: [10.1038/s41591-019-0392-8](https://doi.org/10.1038/s41591-019-0392-8); pmid: [30886409](#)
84. H. Li *et al.*, The Sequence Alignment/Map format and SAMtools. *Bioinformatics* **25**, 2078–2079 (2009). doi: [10.1093/bioinformatics/btp352](https://doi.org/10.1093/bioinformatics/btp352); pmid: [19505943](#)
85. B. Langmead, S. L. Salzberg, Fast gapped-read alignment with Bowtie 2. *Nat. Methods* **9**, 357–359 (2012). doi: [10.1038/nmeth.1923](https://doi.org/10.1038/nmeth.1923); pmid: [22388286](#)
86. M. J. Mina *et al.*, Measles virus infection diminishes preexisting antibodies that offer protection from other pathogens. *Science* **366**, 599–606 (2019). doi: [10.1126/science.aay6485](https://doi.org/10.1126/science.aay6485); pmid: [31672891](#)
87. S. Chevrier *et al.*, Compensation of signal spillover in suspension and imaging mass cytometry. *Cell Syst.* **6**, 612–620.e5 (2018). doi: [10.1016/j.cels.2018.02.010](https://doi.org/10.1016/j.cels.2018.02.010); pmid: [29605184](#)
88. J. H. Levine *et al.*, Data-driven phenotypic dissection of AML reveals progenitor-like cells that correlate with prognosis. *Cell* **162**, 184–197 (2015). doi: [10.1016/j.cell.2015.05.047](https://doi.org/10.1016/j.cell.2015.05.047); pmid: [26095251](#)
89. G. X. Y. Zheng *et al.*, Massively parallel digital transcriptional profiling of single cells. *Nat. Commun.* **8**, 14049 (2017). doi: [10.1038/ncomms14049](https://doi.org/10.1038/ncomms14049); pmid: [28091601](#)
90. Satija Lab, PBMC CITE-seq reference, version 1.0.0, Zenodo (2023); <https://doi.org/10.5281/zenodo.7779017>.
91. Y. Hao *et al.*, Integrated analysis of multimodal single-cell data. *Cell* **184**, 3573–3587.e29 (2021). doi: [10.1016/j.cell.2021.04.048](https://doi.org/10.1016/j.cell.2021.04.048); pmid: [34062119](#)
92. G. Korotkevich *et al.*, Fast gene set enrichment analysis. bioRxiv 060012 [Preprint] (2016); <https://doi.org/10.1101/060012>.
93. F. Pedregosa *et al.*, Scikit-learn: Machine learning in Python. *J. Mach. Learn. Res.* **12**, 2825–2830 (2011).
94. S. M. Lundberg, S.-I. Lee, A unified approach to interpreting model predictions. arXiv1705.07874 [cs.AI] (2017).
95. Y. Benjamini, Y. Hochberg, Controlling the false discovery rate: A practical and powerful approach to multiple testing. *J. R. Stat. Soc. B* **57**, 289–300 (1995). doi: [10.1111/j.2517-6161.1995.tb02031.x](https://doi.org/10.1111/j.2517-6161.1995.tb02031.x)
96. M. Friendly, Corrrgrams: Exploratory displays for correlation matrices. *Am. Stat.* **56**, 316–324 (2002). doi: [10.1198/000313002533](https://doi.org/10.1198/000313002533)
97. A. Kuznetsova, P. B. Brockhoff, R. H. B. Christensen, lmerTest Package: Tests in linear mixed effects models. *J. Stat. Softw.* **82**, 1–26 (2017). doi: [10.18637/jss.v082.i03](https://doi.org/10.18637/jss.v082.i03)
98. H. Wickham *et al.*, Welcome to the Tidyverse. *J. Open Source Softw.* **4**, 1686 (2019). doi: [10.21105/joss.01686](https://doi.org/10.21105/joss.01686)
99. S. Seabold, J. Perktold, “Statsmodels: Econometric and Statistical Modeling with Python,” SciPy 2010, 9th Python in Science Conference, Austin, Texas, 28 to 30 June 2010, pp. 92–96; <https://doi.org/10.25080/Majora-92bf1922-011>.
100. E. von Elm *et al.*, Strengthening the Reporting of Observational Studies in Epidemiology (STROBE) statement: Guidelines for reporting observational studies. *BMJ* **335**, 806–808 (2007). doi: [10.1136/bmj.39335.541782.AD](https://doi.org/10.1136/bmj.39335.541782.AD); pmid: [17947786](#)
101. C. Cervia-Hasler, S. Brueningk, T. Hoch, Persistent complement dysregulation with signs of thromboinflammation in active Long Covid, version 1, Mendeley Data (2024); <https://doi.org/10.17632/dvf6yvrg4x.1>.
102. S. Brueningk, BorgwardtLab/LongCOVID: First Release, version v0, Zenodo (2023); <https://doi.org/10.5281/zenodo.10022438>.
103. Mount Sinai COVID-19 Biobank data, Synapse (2022); <https://www.synapse.org/#/Synapse:syn35874390/>.
- ACKNOWLEDGMENTS**
We thank J. Muri, D. Robbiani, V. Cecchinato, M. Uggioni, A. Guaita, E. Bächli, A. Rudiger, M. Stüssi-Helbling, and L. Huber; all members of the Mount Sinai COVID-19 Biobank Team; the SomaLogic team, including K. Jenko, L. Vahlkamp, and E. Zepko; and the Functional Genomics Center Zurich, including N. Falko; and all members of the Boyman laboratory for their support, particularly A. Maier. Details about institutional review board approvals and informed patient consent can be found in the materials and methods. **Funding:** Swiss National Science Foundation (NRP 78 Implementation Programme to C.C.-H. and O.B.; 4078PO-198431 to O.B. and J.N.; 310030-200669 and 310030-212240 to O.B.), Clinical Research Priority Program CYTImm-Z of UZH (to O.B.), Pandemic Fund of UZH (to O.B.), Innovation grants of University Hospital Zurich (USZ) (to O.B., A.A., and M.E.), Digitalization Initiative of Zurich Higher Education Institutions Rapid-Action Call 2021.1_RAC_ID_34 (to C.C.-H.), Swiss Academy of Medical Sciences (SAMW) fellowships (323530-191220 to C.C.-H.; 323530-191230 to Y.Z.; 323530-177975 to S.A.), Young Talents in Clinical Research project grant (YTCR 08/20) by SAMW and Baugarter Foundation (to M.E.R.), Filling the Gap Program of UZH (to M.E.R.), UZH Postdoc Grant (FK-22-053 to D.M.), Botnar Research Centre for Child Health Postdoctoral Excellence Programme (#PEP-2021-1008 to S.C.B.), and European Union’s Horizon 2020 research and innovation program under the Marie Skłodowska-Curie grant agreement (813533 to K.B., B.F., and G.M.; 801076 to T.B.), Driver Grant 2017DR17 of Swiss Personalized Health Network (to A.A. and M.E.), NOMIS Foundation, Schwyzer Winiker Stiftung and Baugarten Stiftung (coordinated by USZ Foundation, USZF27101, to A.A. and M.E.), and the Swiss canton of Grisons (to C.B.M.). **Author contributions:** Conceptualization: C.C.-H. and O.B. Methodology: C.C.-H., S.C.B., K.B., and O.B. Investigation: C.C.-H., S.C.B., T.H., B.F., G.M., R.C.T., L.C., R.M., P.W., M.E., P.T., Y.Z., M.P., D.M., T.B., S.C.-H., S.A., M.M., A.W.C., M.P., P.B., J.N., A.A., M.E.R., C.B.M., N.D.B., K.B., and O.B. Visualization: C.C.-H. and O.B. Funding acquisition: C.C.-H., Y.Z., S.A., M.E.R., J.N., and O.B. Project administration: S.C. and M.E.R. Supervision: K.B. and O.B. Writing: C.C.H. and O.B. **Competing interests:** C.B.M. works as an adviser for Elliptica Ltd. C.C.-H., S.C.B., B.F., G.M., K.B., and O.B. are listed as inventors on a patent application on biomarkers in Long Covid. The other authors declare that they have no competing interests. **Data and materials availability:** All data needed to evaluate the conclusions in the paper are present in the paper or the supplementary materials or have been deposited at Mendeley ([101](#)) or Zenodo ([102](#)). Replication data were obtained directly from the authors of previously published work ([24](#)). Researchers can access the Mount Sinai COVID-19 Biobank data on Synapse ([103](#)) by registering for a free account (Synapse project ID syn35874390). There are no restrictions on access or use of these datasets. **License information:** Copyright © 2024 the authors, some rights reserved; exclusive licensee American Association for the Advancement of Science. No claim to original US government works. <https://www.science.org/about/science-licenses-journal-article-reuse>. This research was funded in whole or in part by the Swiss National Science Foundation (4078PO-198431, 310030-200669, 310030-212240) and the European Union’s Horizon 2020 research and innovation program under the Marie Skłodowska-Curie grant agreement (813533 and 801076), cOAIIion S organizations. The author will make the Accepted Manuscript (AAM) version available under a CC BY public copyright license.
- SUPPLEMENTARY MATERIALS**
science.org/doi/10.1126/science.adg7942
Figs. S1 to S8
Tables S1 to S5
STROBE Checklist
MDAR Reproducibility Checklist
Data S1 to S9
- Submitted 21 January 2023; resubmitted 1 September 2023
Accepted 24 November 2023
10.1126/science.adg7942